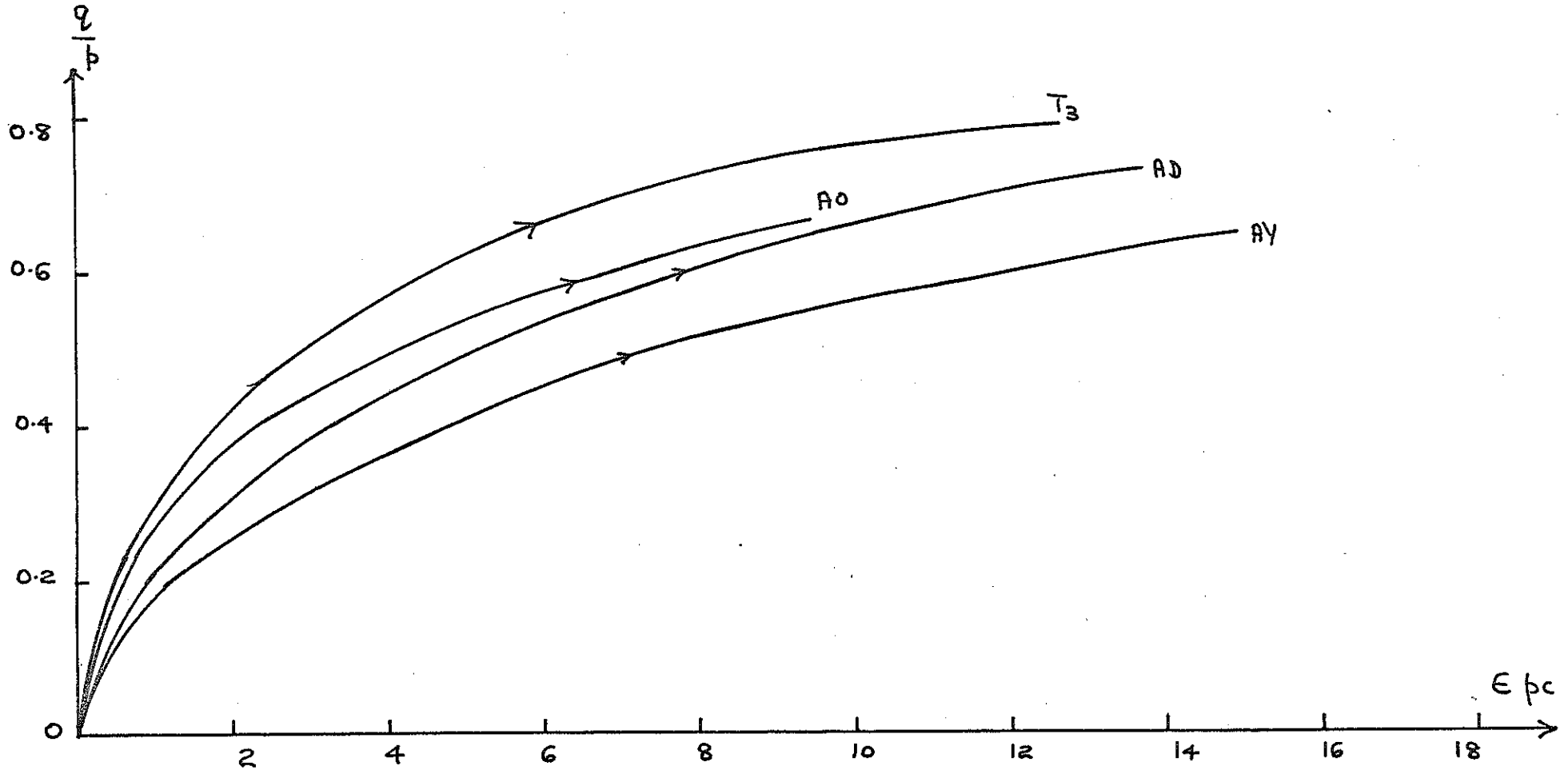

Fig. 7.5 The $(\frac{q}{p}, \epsilon)$ characteristics of specimens T_3, AO, AD and AY sheared along group I test paths from 90 psi isotropic stress.

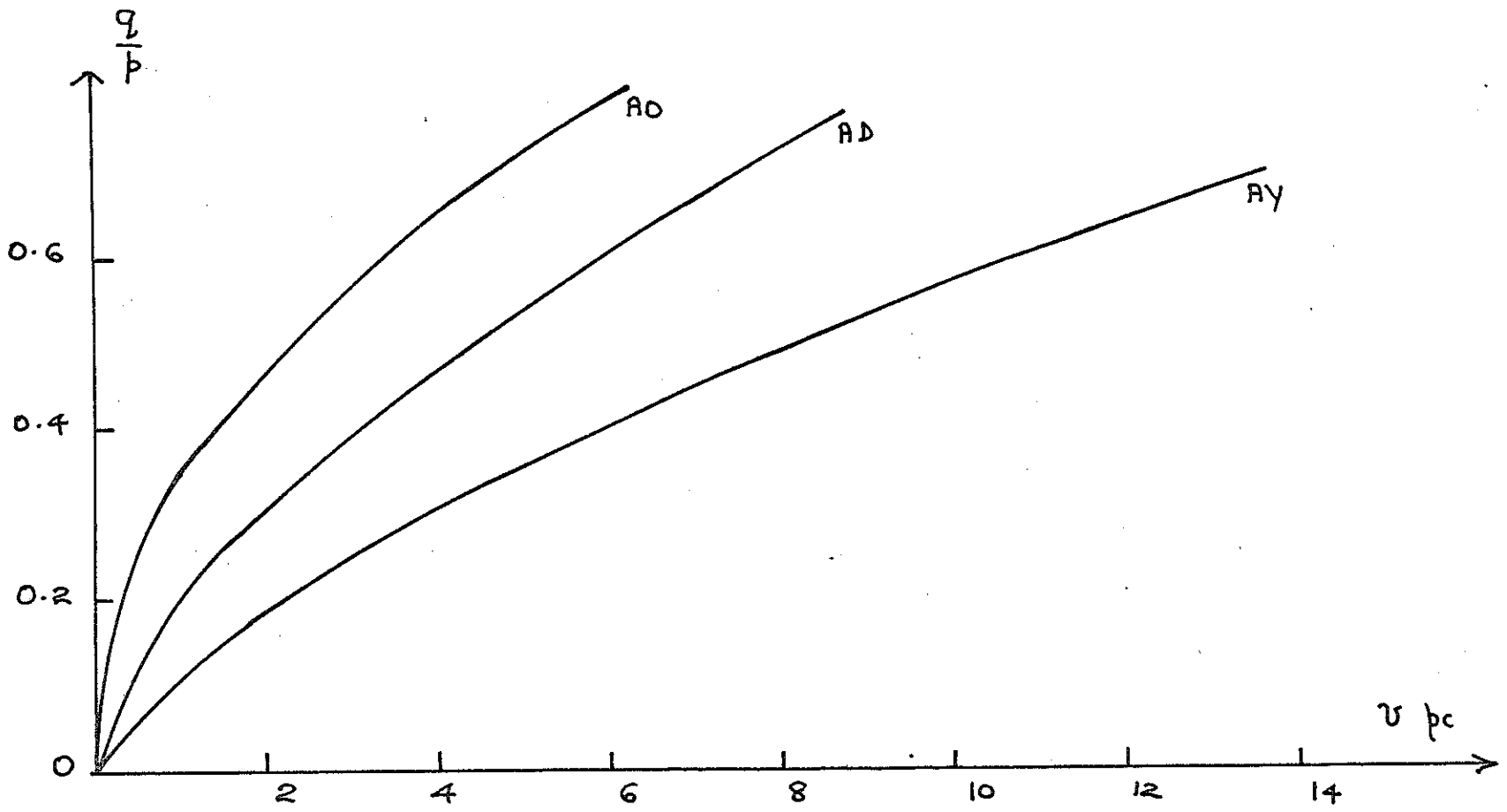

Fig. 7.6 The $(\frac{q}{p}, v)$ characteristics of specimens AO, AD and AY sheared along Group I test paths from 90 psi isotropic stress.

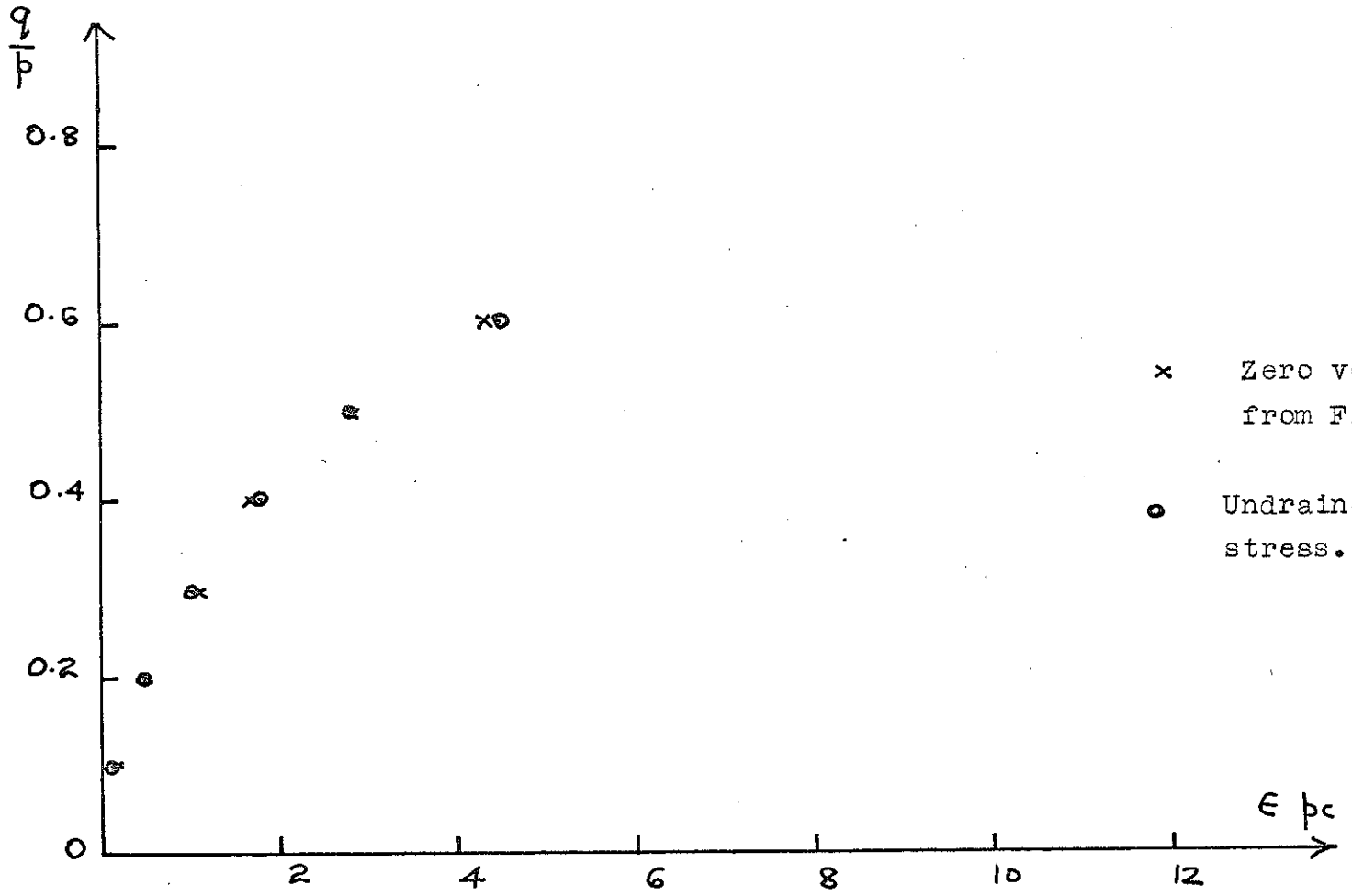

Fig. 7.7. The $(\frac{q}{p}, \epsilon)$ characteristic of the undrained test T_3 and the zero volumetric strain projection of the constant q/p contours from Fig. 7.3

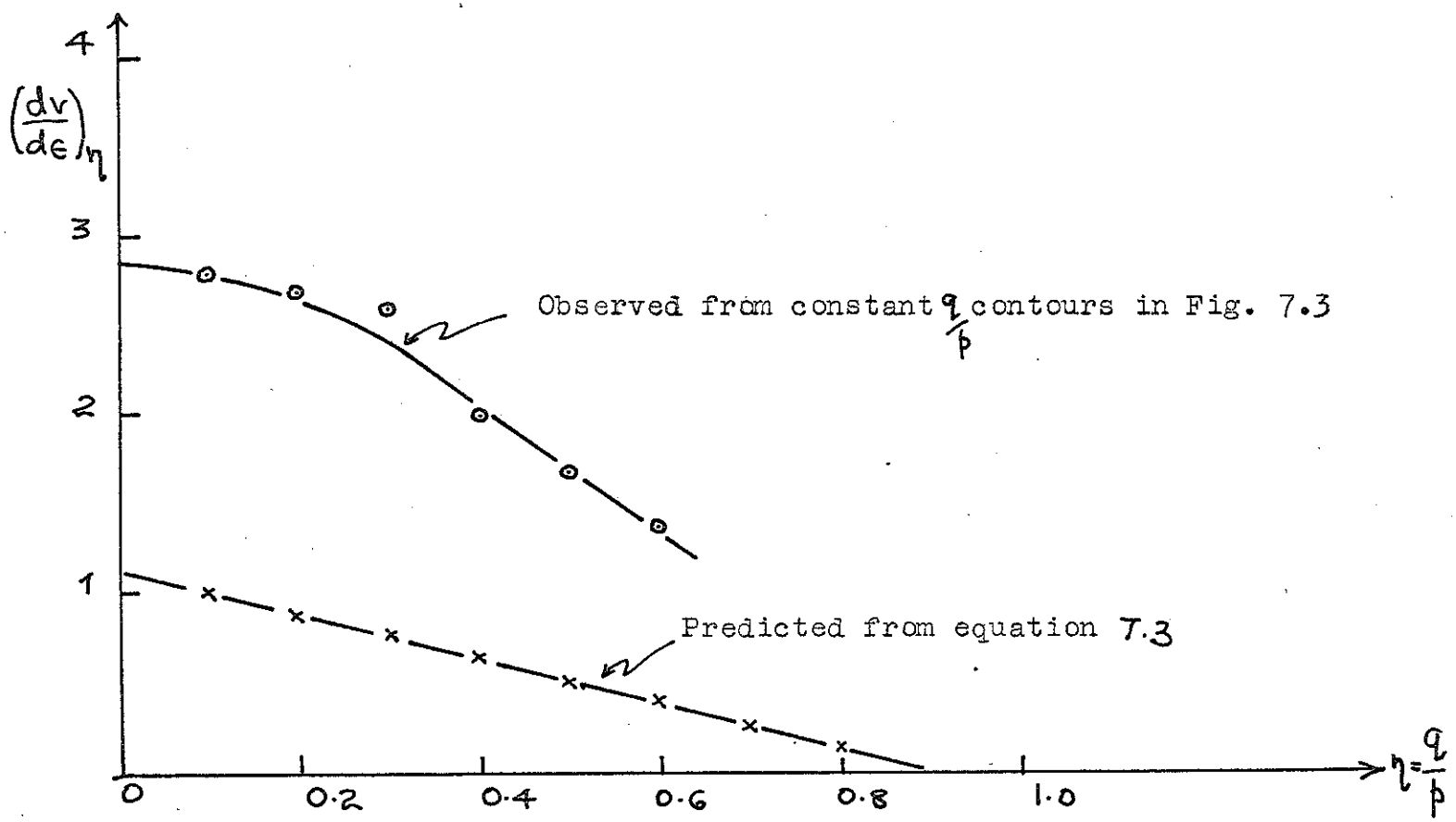

Fig.7.8. The slope of constant q/p contours in (υ , ϵ) space from fig.7.3 and the $\left(\frac{dv}{d\epsilon}\right)_\eta$ predicted from the energy equation of Wroth (1965).

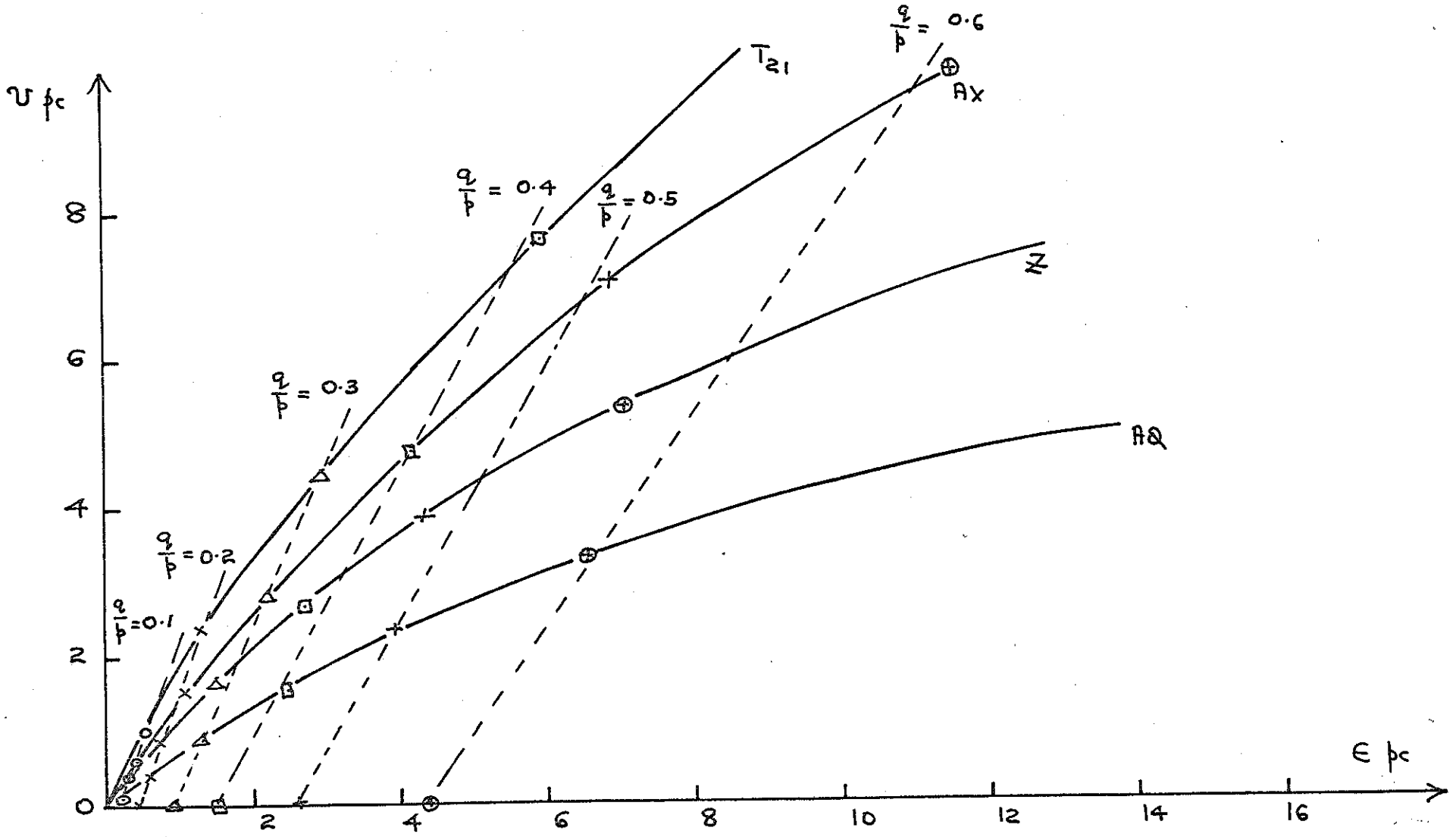

Fig. 7.9 Constant q/p contours on the (υ, ϵ) characteristics of specimens T_{21}, AX, Z and AQ. sheared from an isotropic stress of 60 psi.

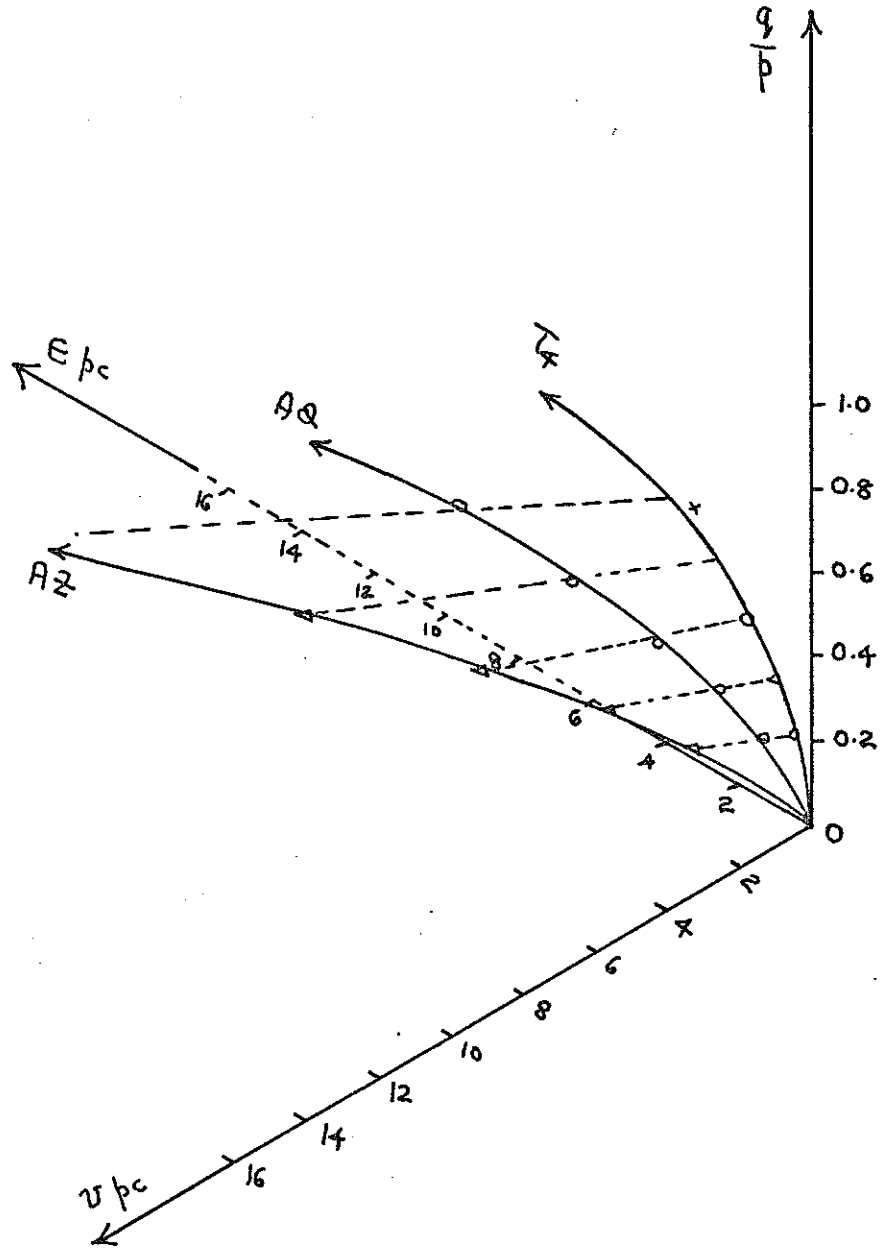

Fig. 7.10. The paths followed by specimens T_4, AQ and Z in the $(\frac{q}{p}, \upsilon, \epsilon)$ space

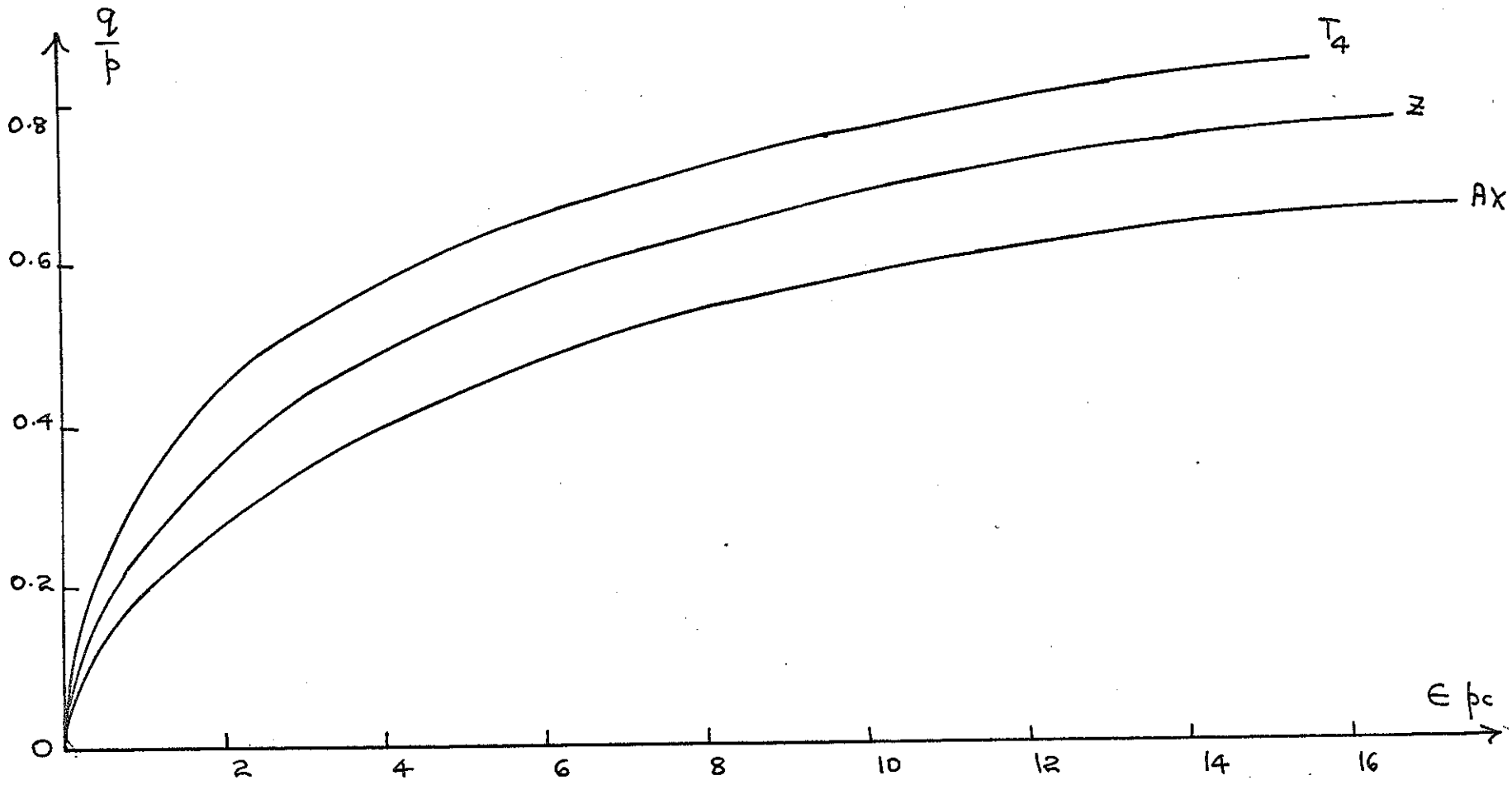

Fig. 7.11 The $(\frac{q}{p}, \epsilon)$ characteristics of specimens T_4, Z and AX sheared from an isotropic stress of 60 psi.

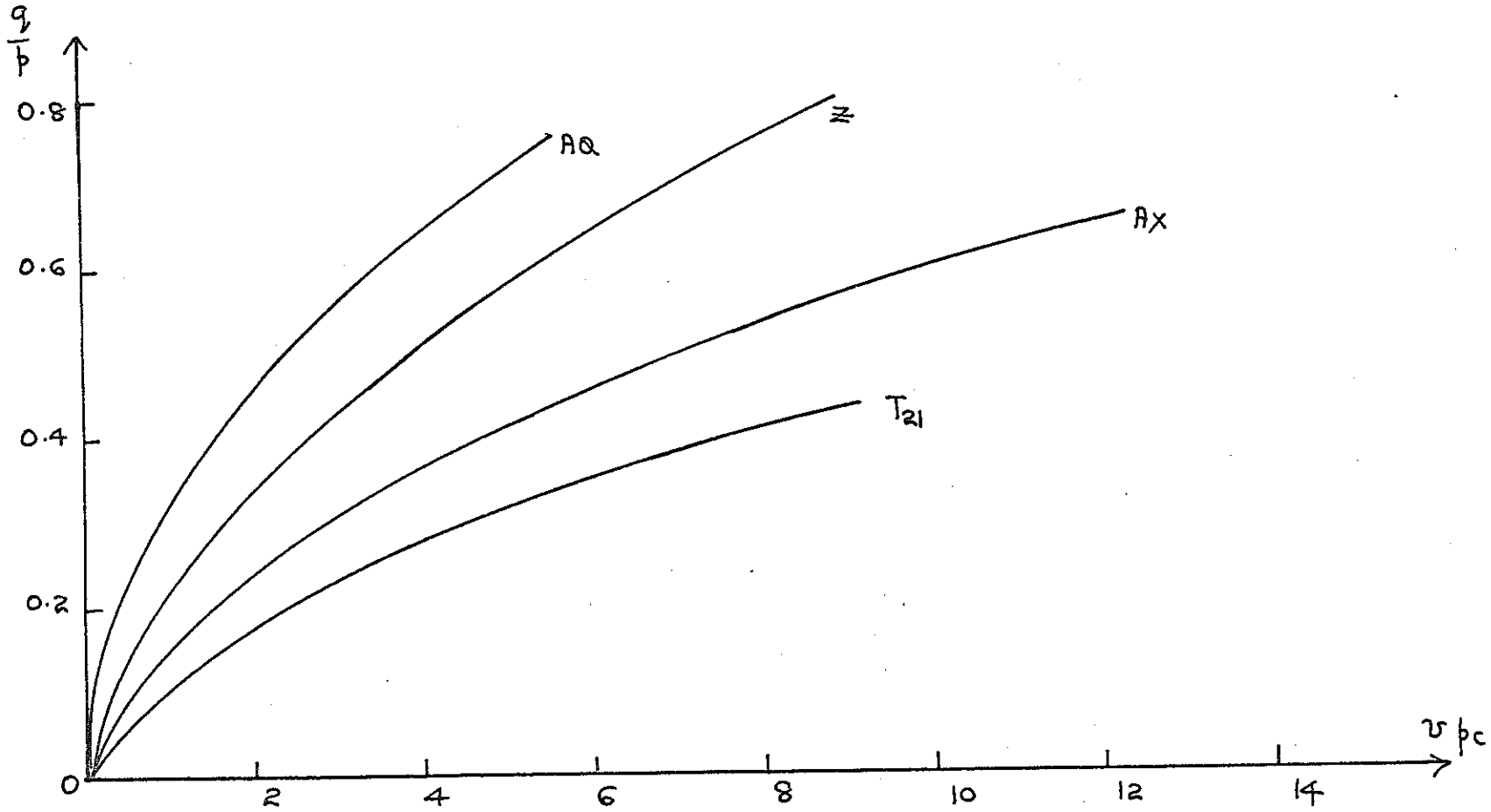

Fig. 7.12 The $(\frac{q}{p}, \upsilon)$ characteristics of specimens AQ, Z, AX and T_{2I} sheared from an isotropic stress of 60 psi.

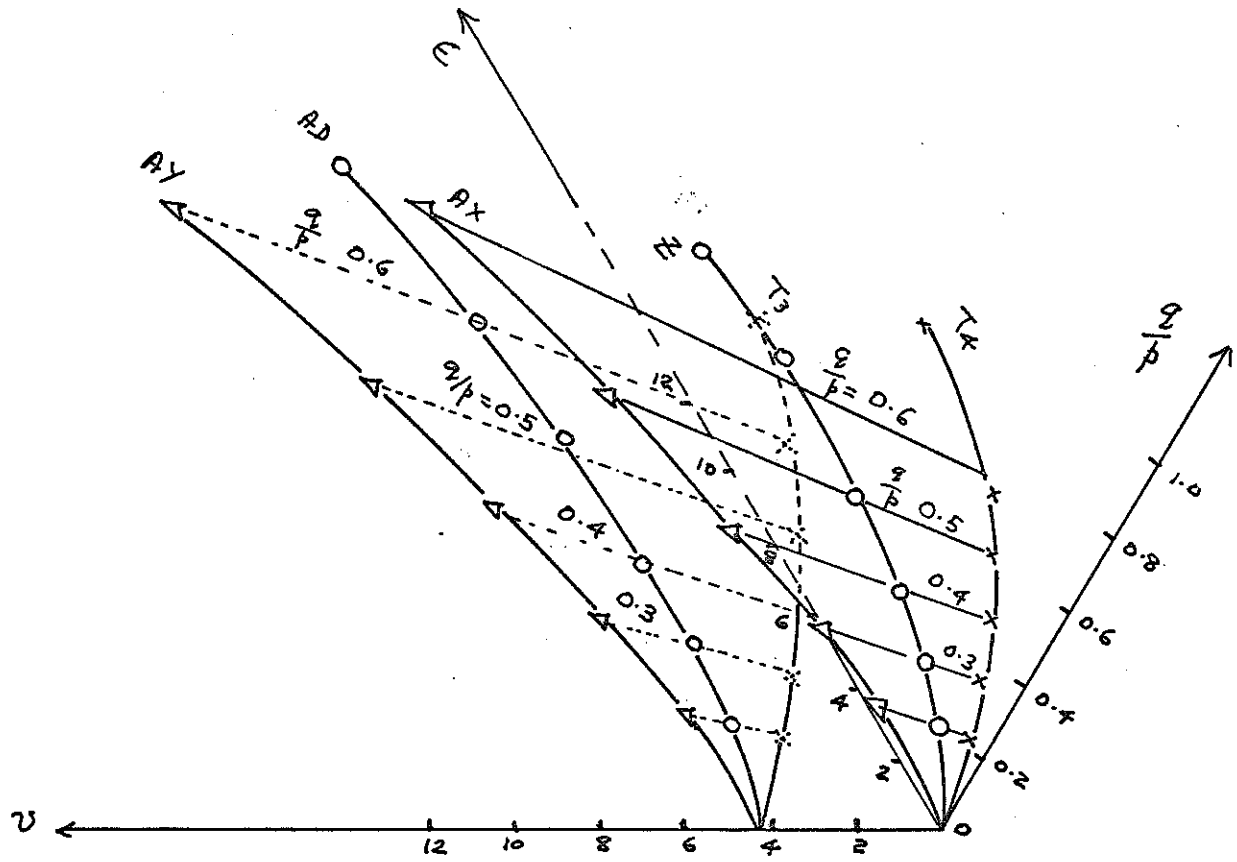

Fig. 7.13 The ($\frac{q}{p}$, v , ϵ) surfaces of specimens sheared along Group 2 stress paths from isotropic stresses of 60 and 90 psi respectively.

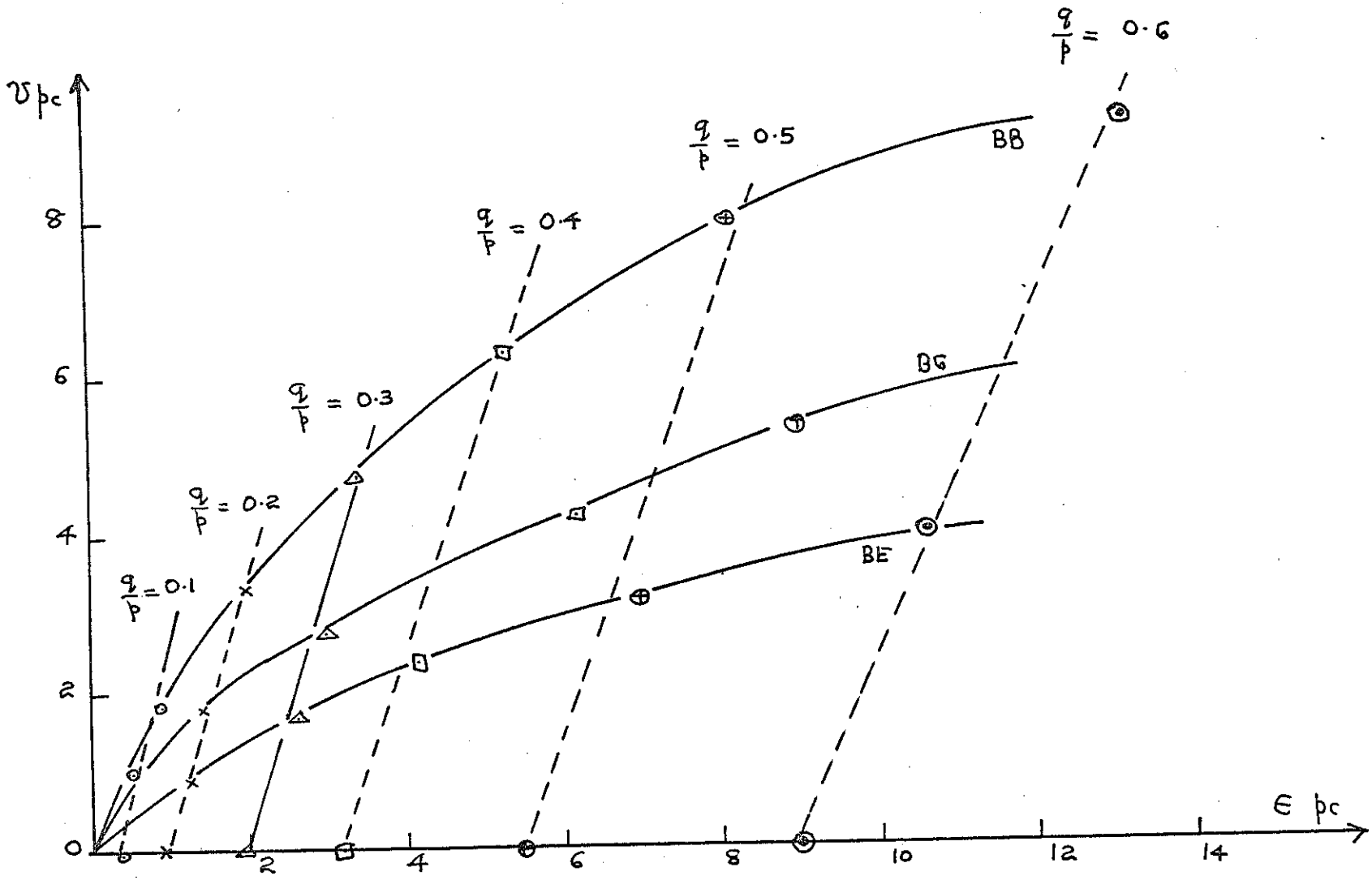

Fig. 7.14. The constant q/p contours on the (υ, ϵ) characteristics of specimens BB, BG, BE and PAL sheared in extension from 60 psi isotropic stress.

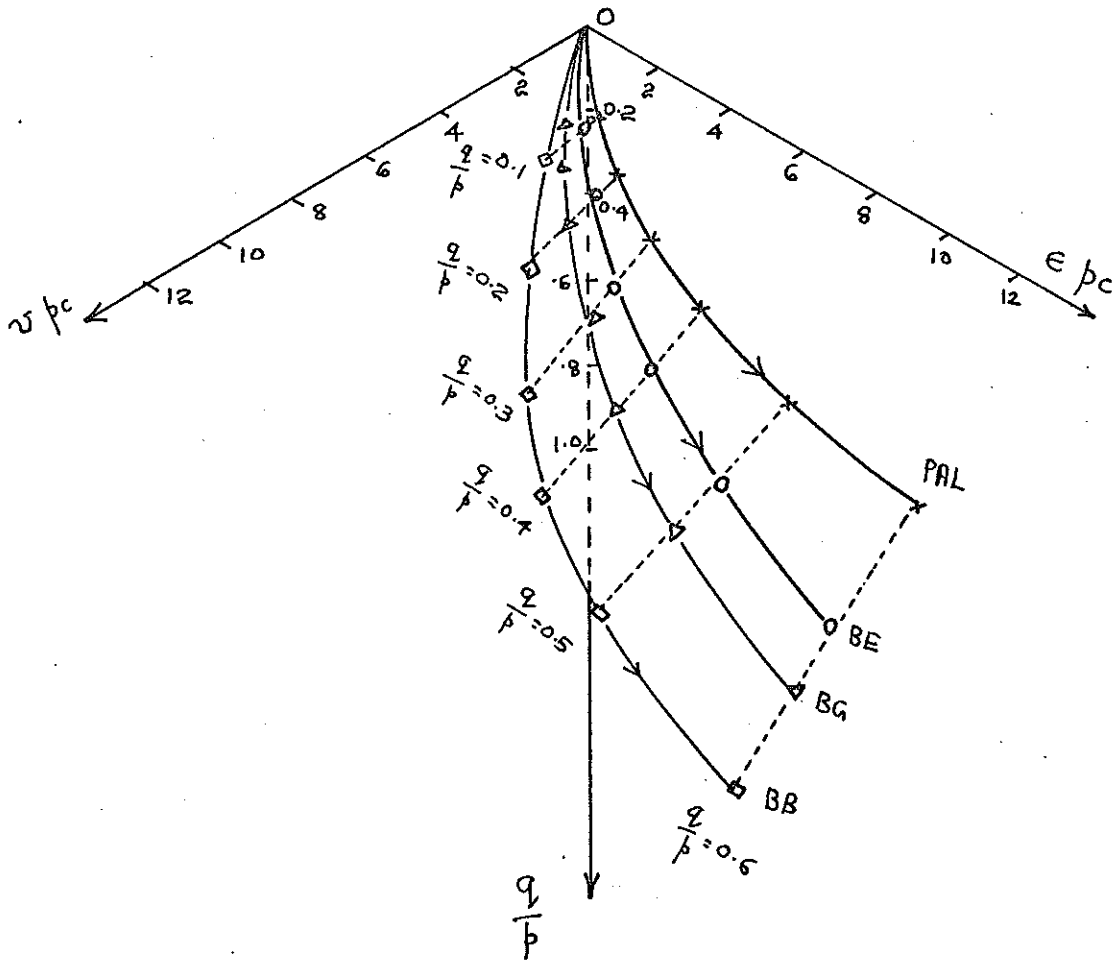

Fig. 7.15. The ($\frac{q}{p}$, υ , ϵ) characteristic of specimens PAL, BE, BG and BB sheared along Group I stress paths in extension.

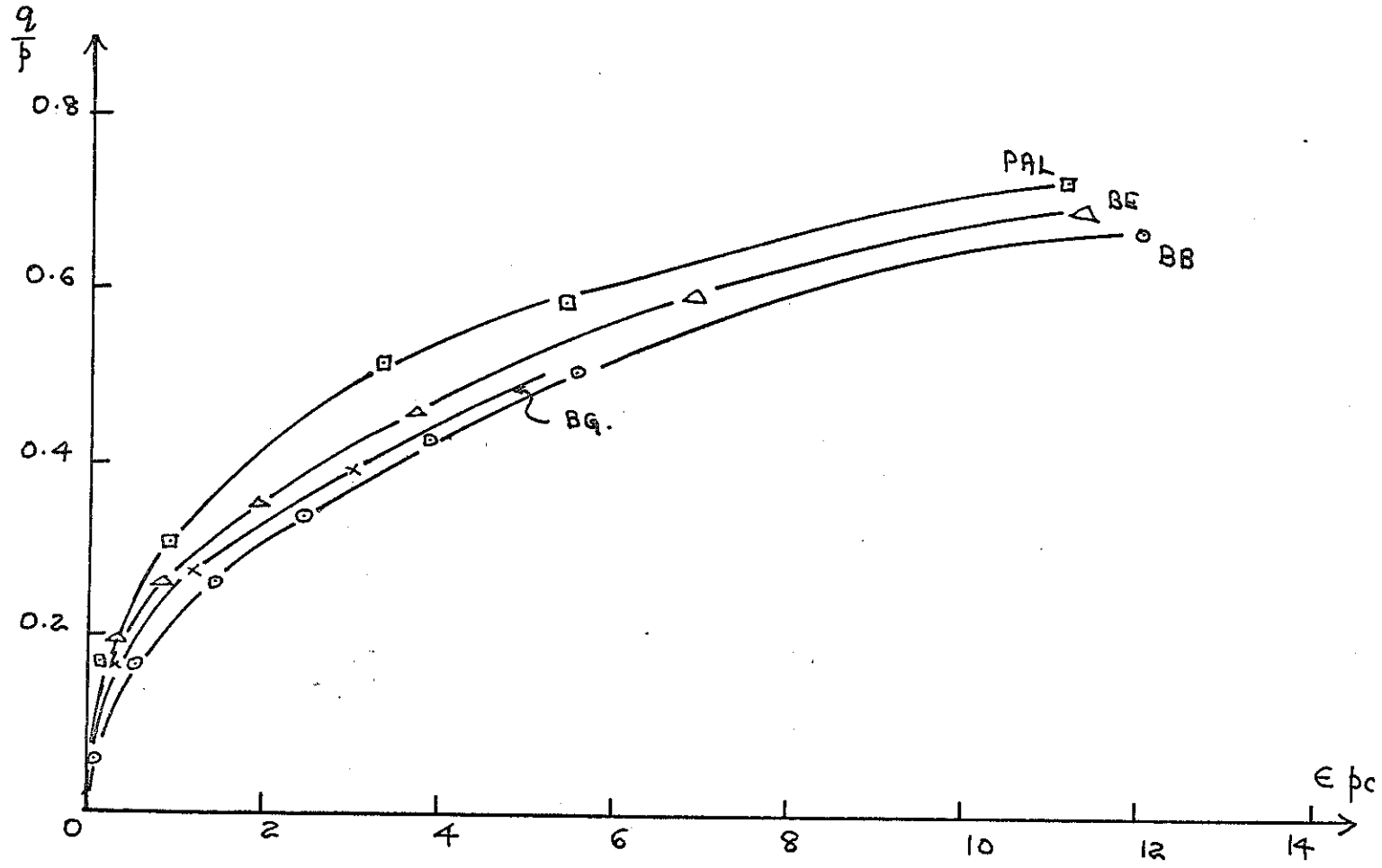

Fig. 7.16 The $(\frac{q}{p}, \epsilon)$ characteristics of specimens BB,BG,BE and PAL sheared in extension from 60 psi isotropic stress.

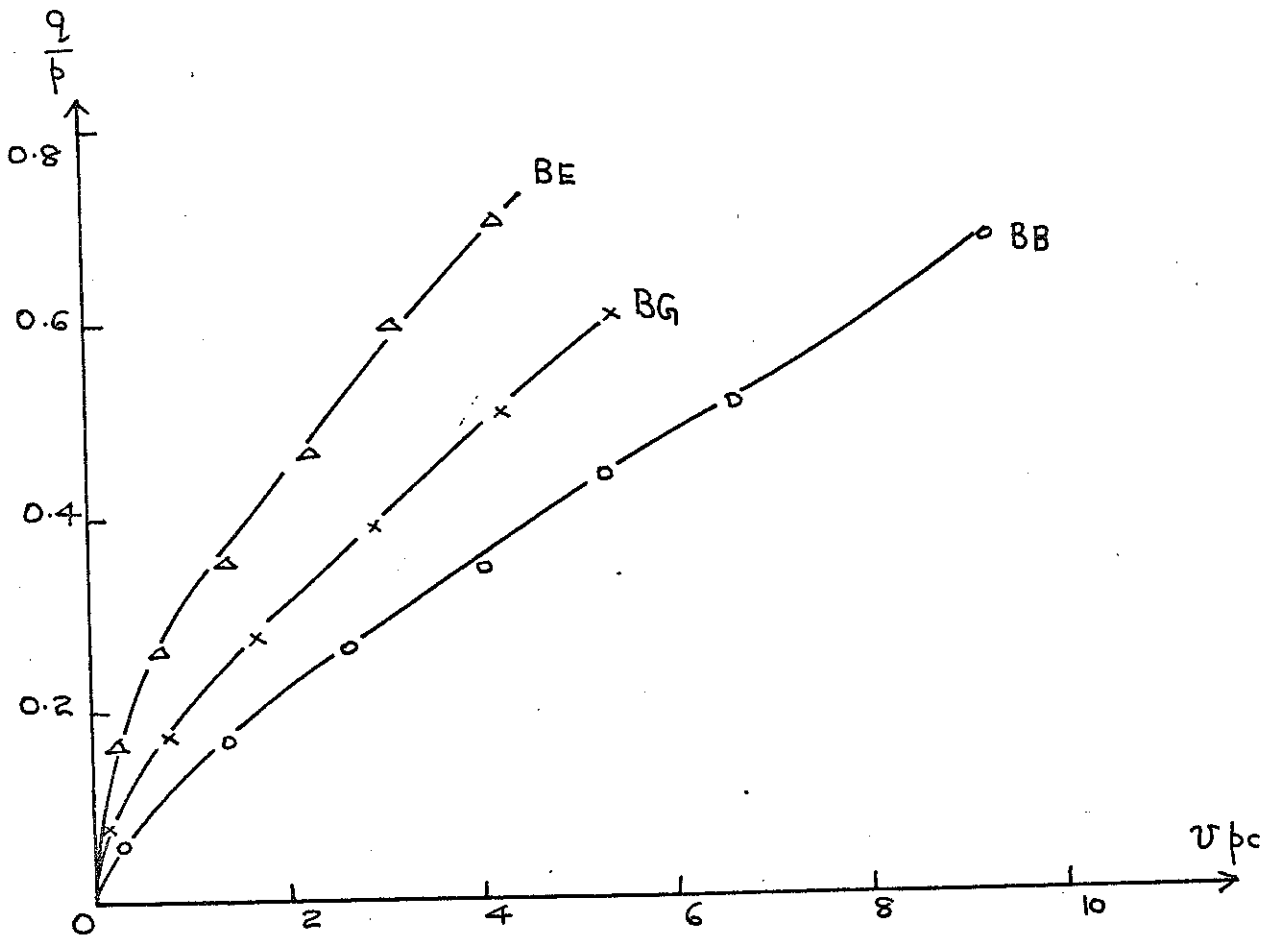

Fig. 7·17. The $(\frac{q}{p}, v)$ characteristics of specimens BB, BE and BG sheared in extension from 60 psi isotropic stress.

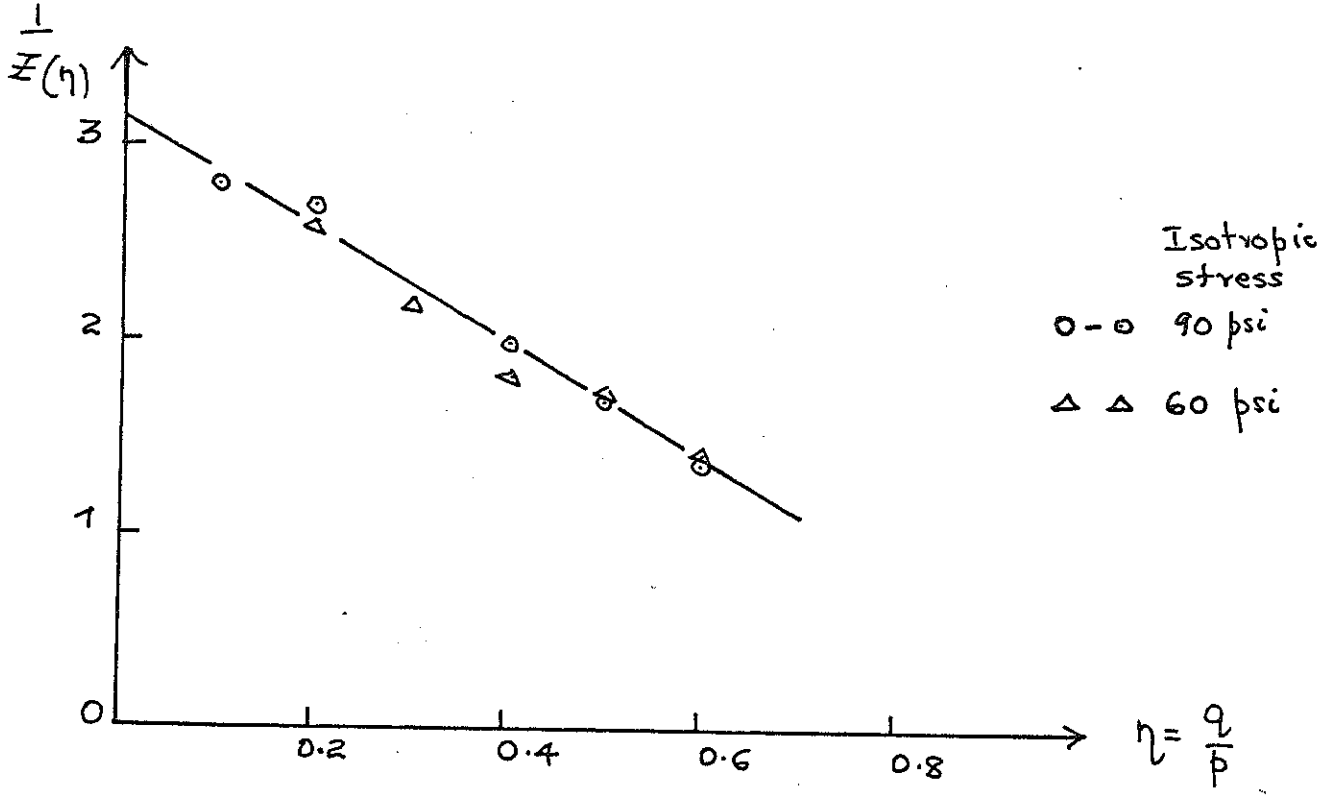

Fig. 7.18. The variation of $\frac{1}{Z}(\eta)$ with η for specimens sheared from 60 and 90 psi isotropic stresses

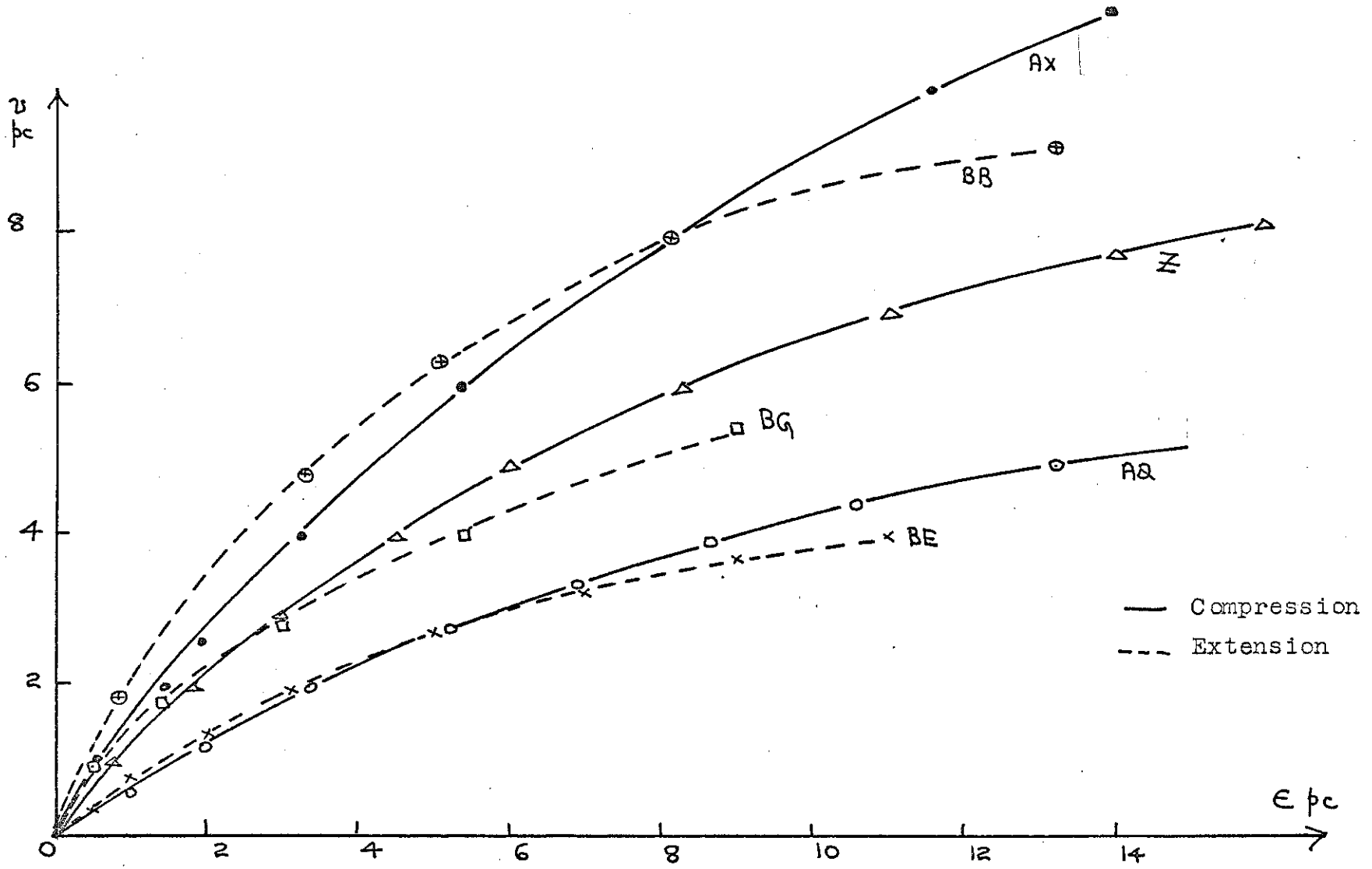

FIG. 7.19. The (υ, ϵ) characteristics of specimens sheared in compression and in extension.

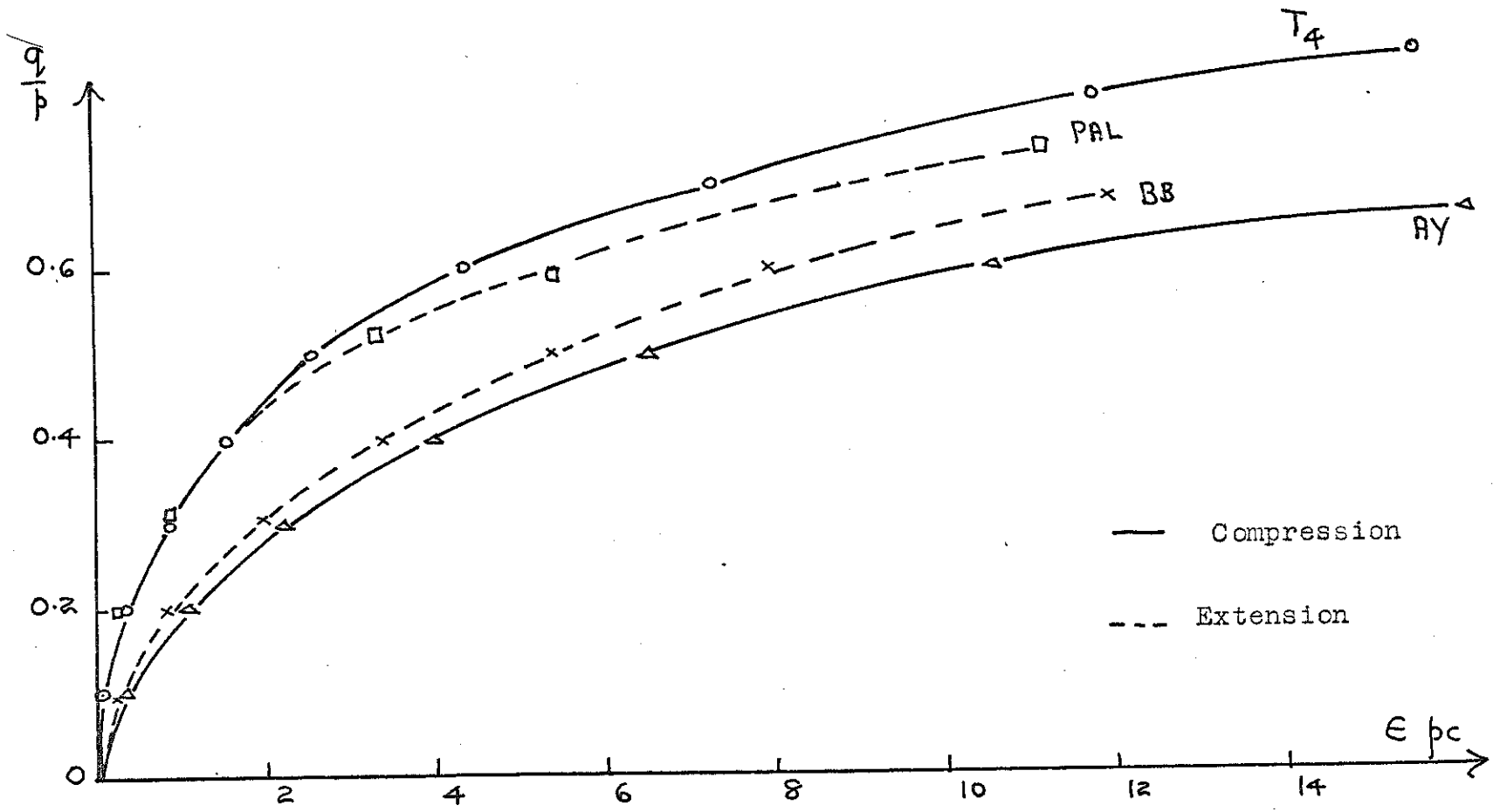

Fig. 7.20. The $(\frac{q}{p}, \epsilon)$ characteristics of specimens sheared in compression and in extension.

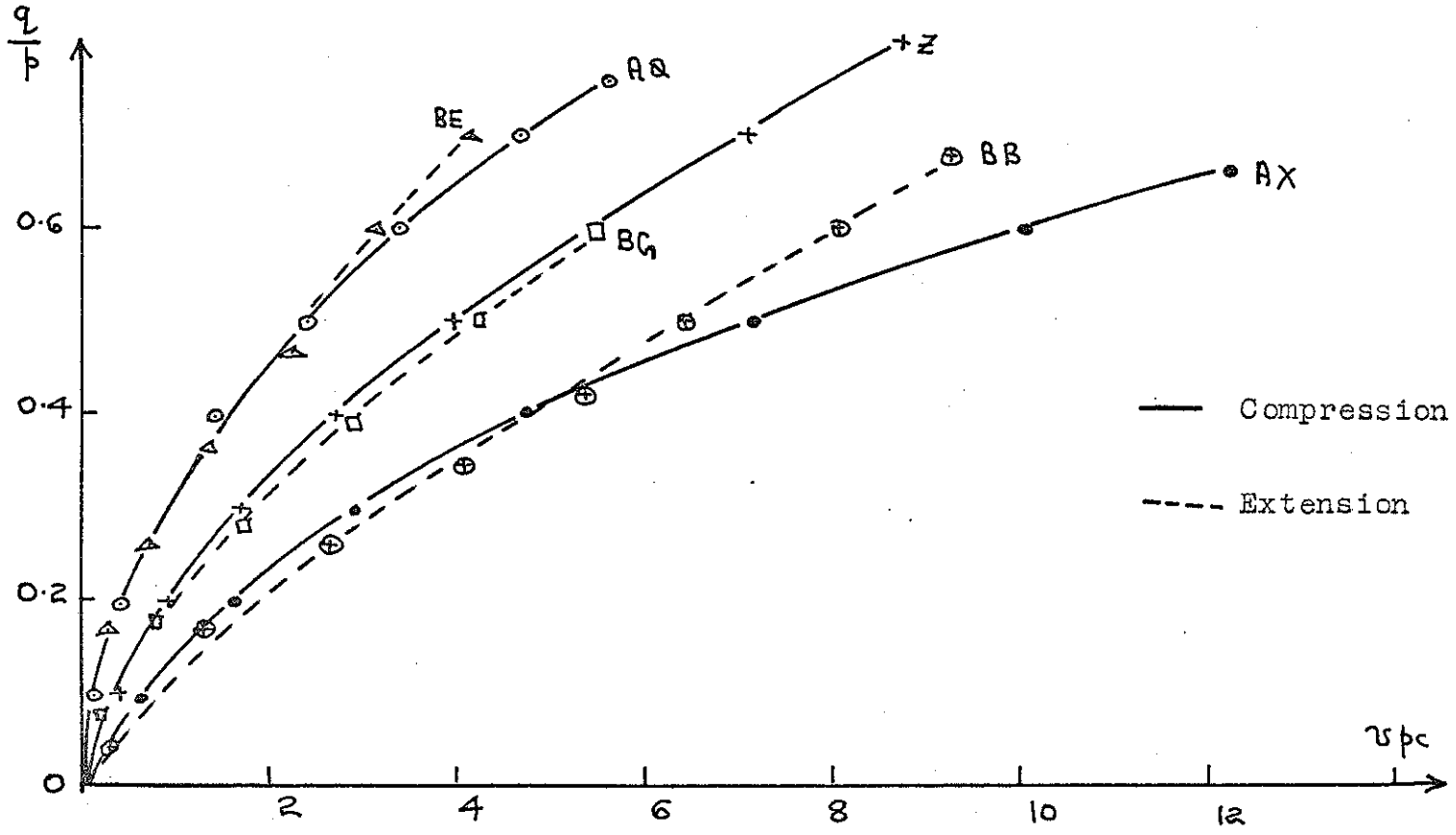

Fig. 7.21 The $(\frac{q}{p}, v)$ characteristics of specimens sheared in compression and in extension.

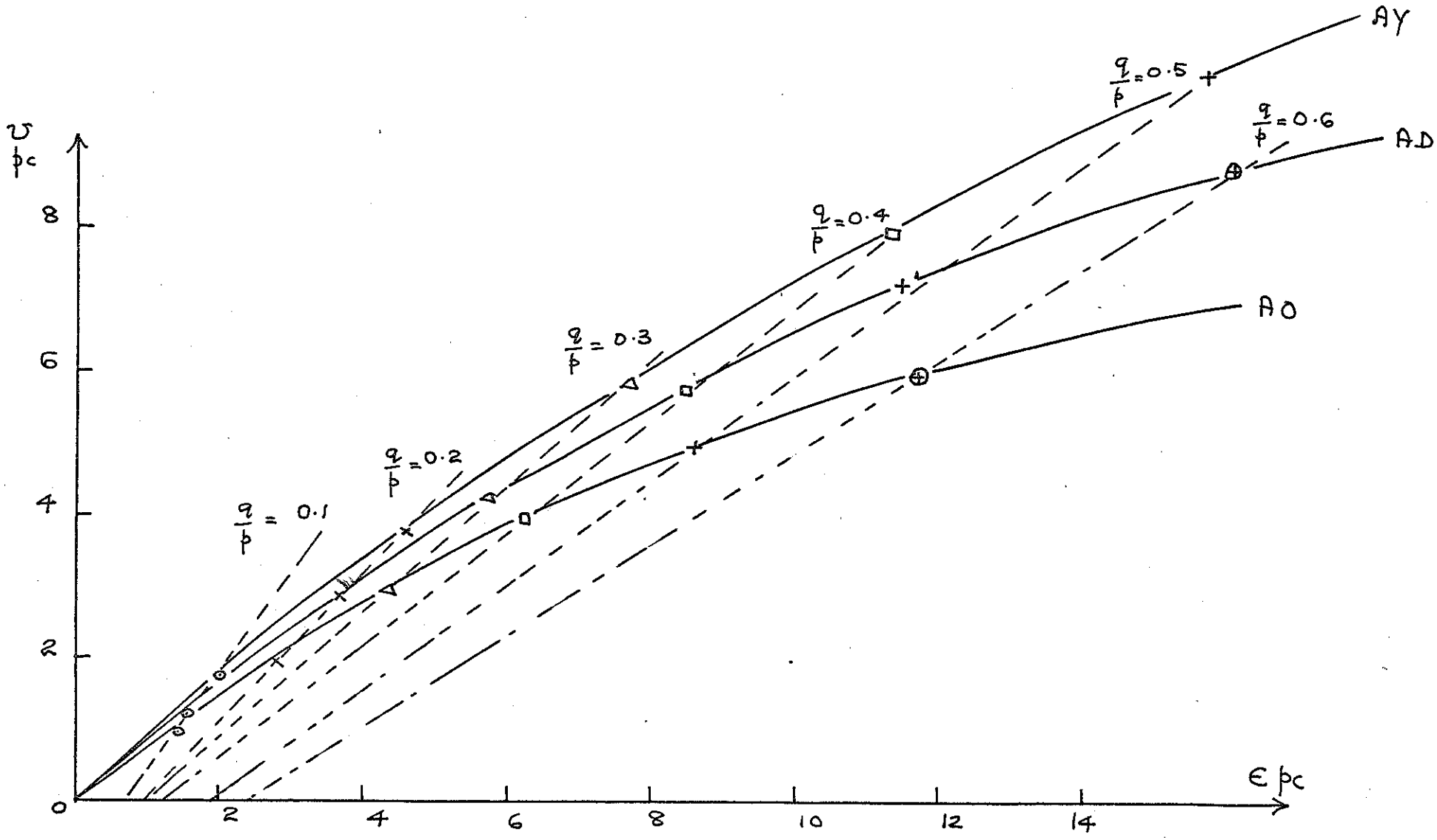

Fig. 7.22. The constant q/p contours on the (v, ϵ) characteristics of specimens AO, AD and AY as predicted from Cam-clay theory.

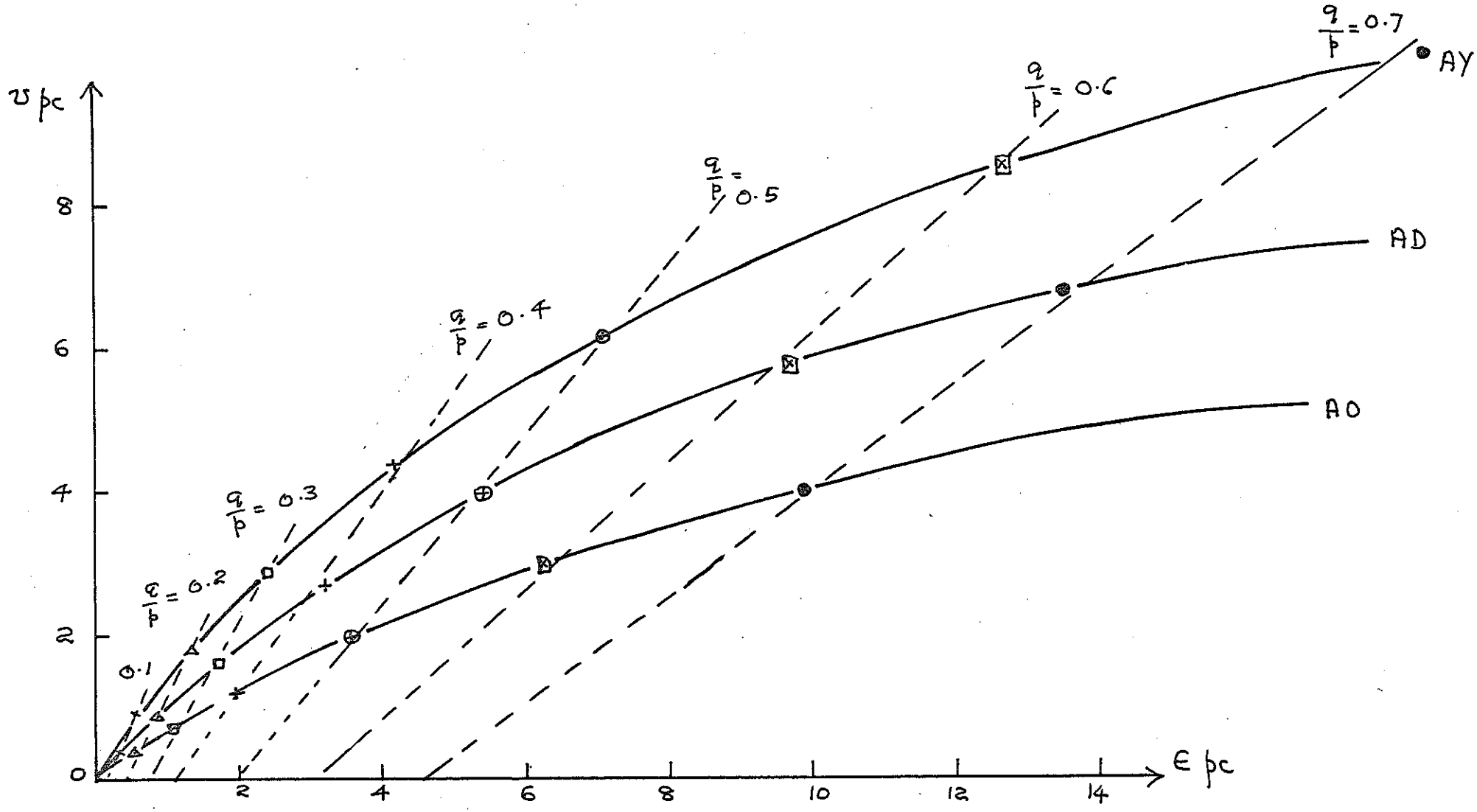

Fig. 7.23. The constant q/p contours on the (υ, ϵ) characteristics of specimens AO, AD and Ay as predicted from the Modified theory.

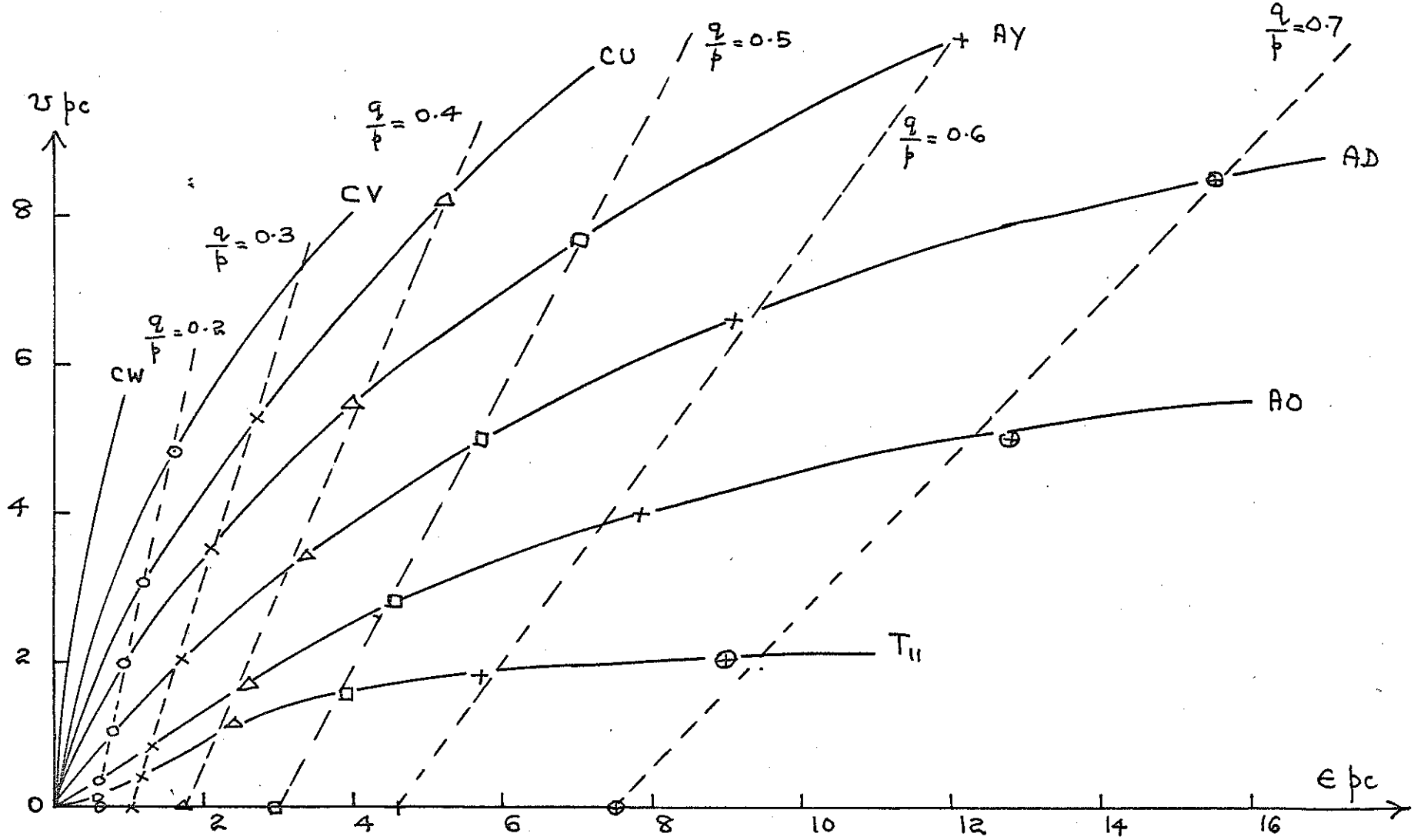

Fig. 7.24. The constant q/p contours on the (υ, ϵ) characteristics of specimens CW, CV, CU, AY, AD, AO and T_{11}, as predicted from the theory of Roscoe and Poorooshasb (1963)

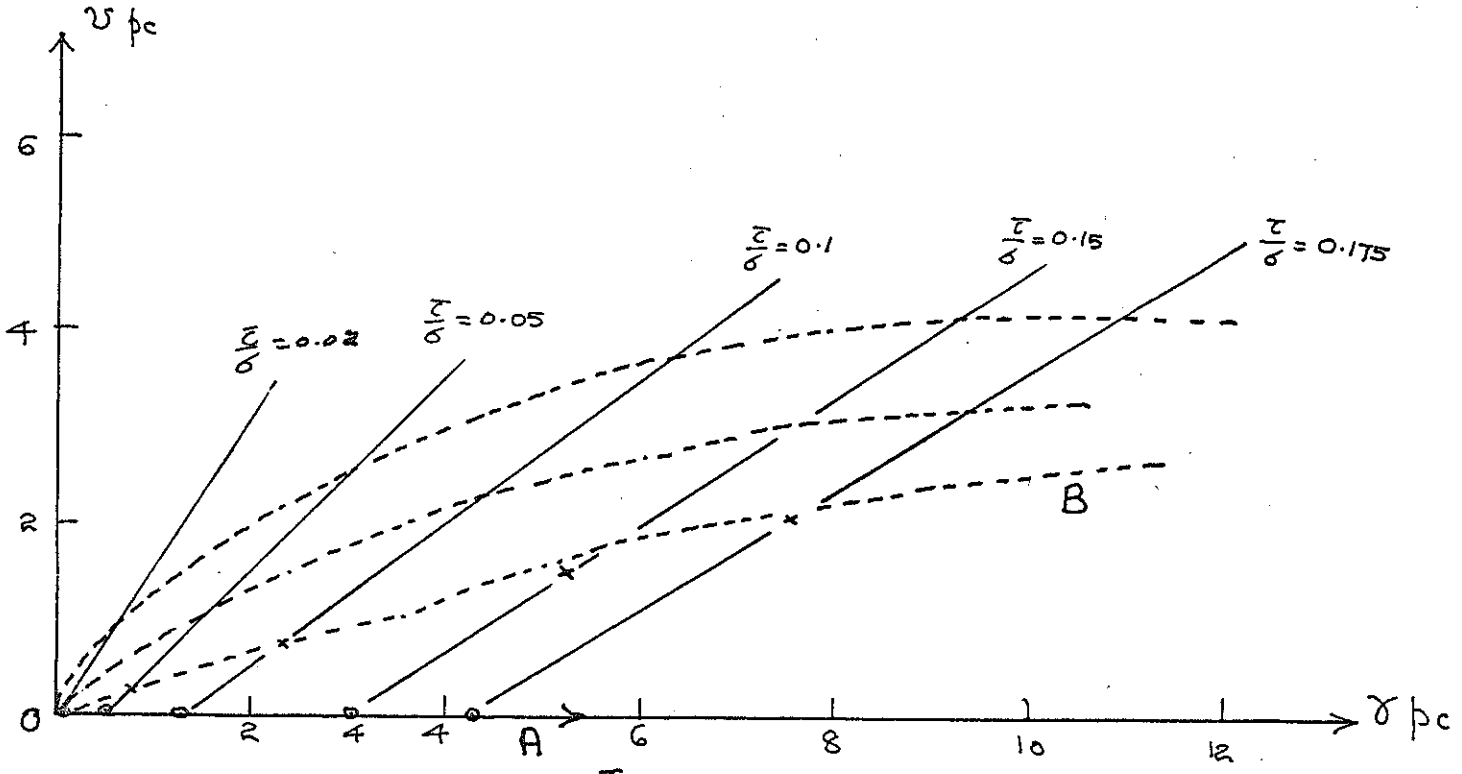

Fig. 7.25. Contours of constant $(\frac{\tau}{\sigma})$ in the (υ, γ) characteristics of specimens sheared in the S.S.A.

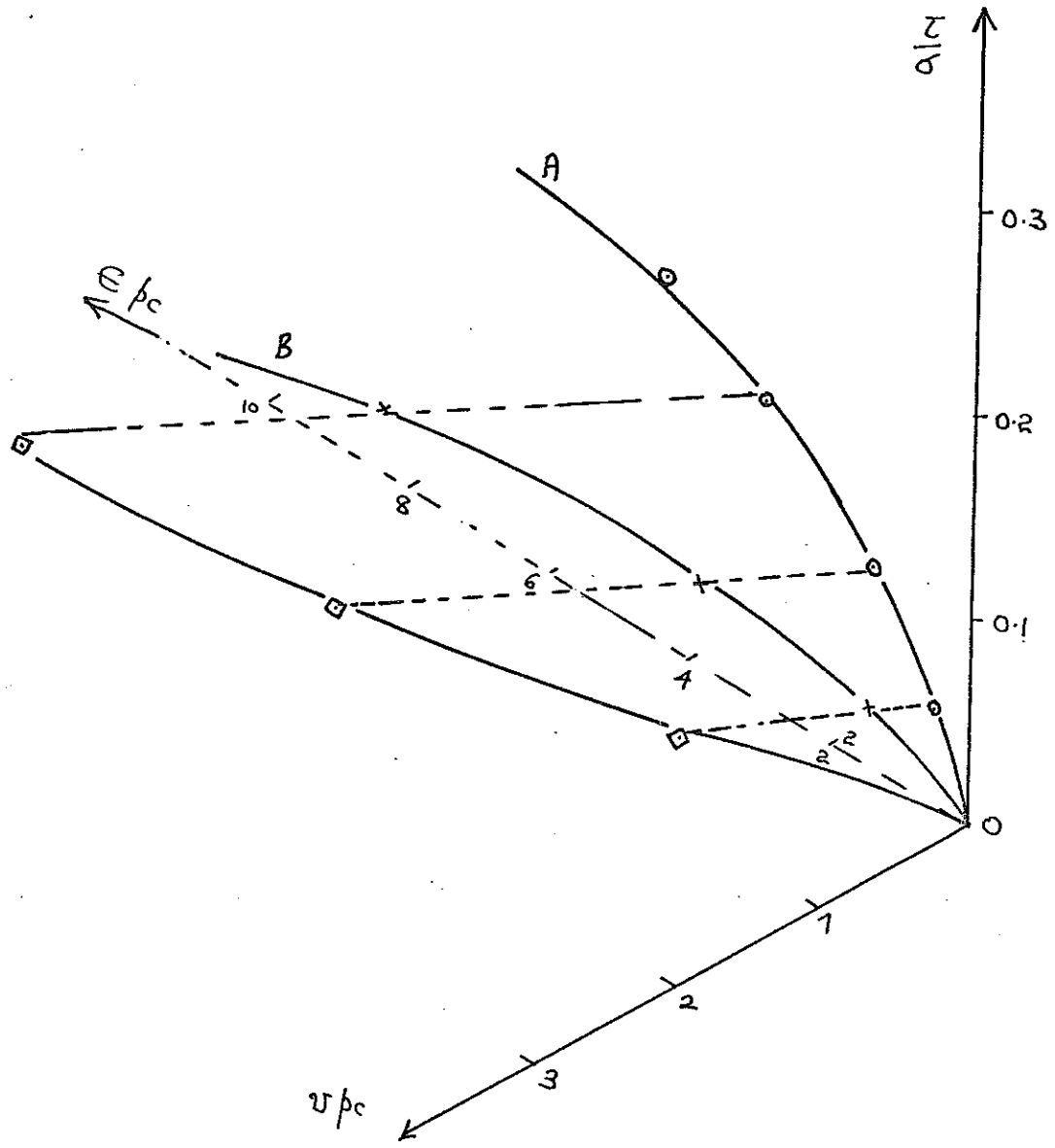

Fig. 7.26. The $(\frac{\tau}{\sigma}, \upsilon, \gamma)$ surface for specimens sheared in the S.S.A. along Group I , test paths.

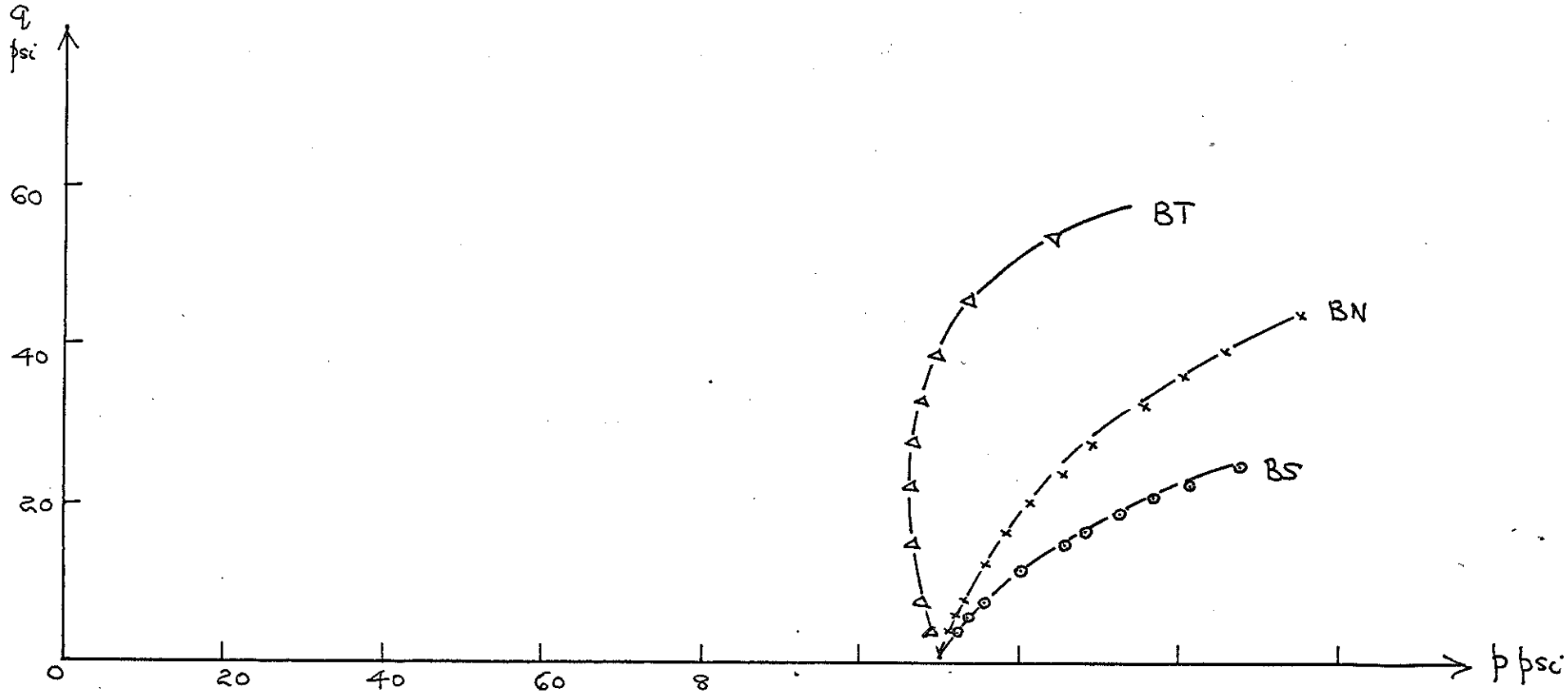

Fig. 7.27. Stress paths of 3 tests BT, BN, and BS with linear strain paths.

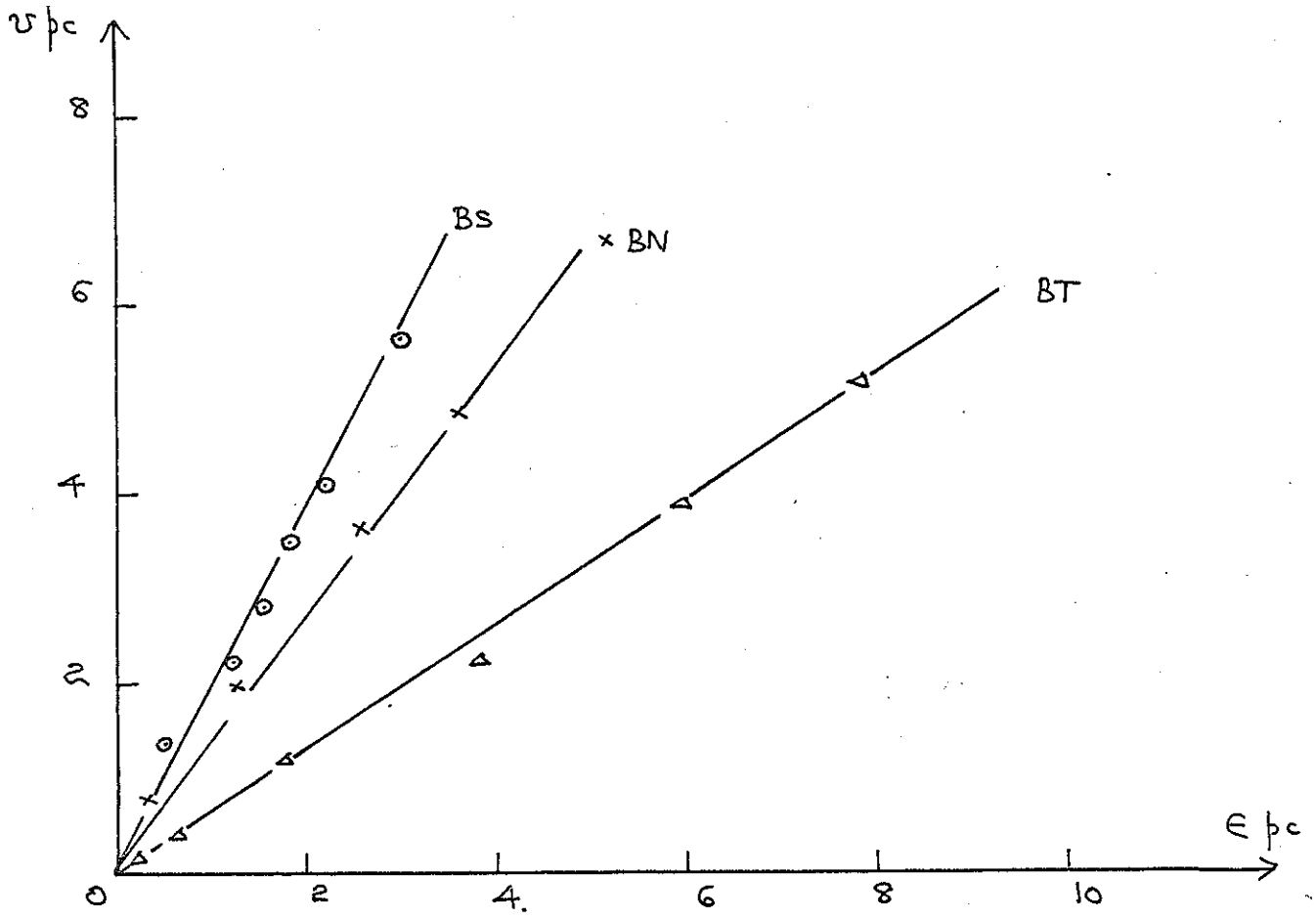

Fig. 7.28. Strain paths for ζ tests BS, BN and BT.

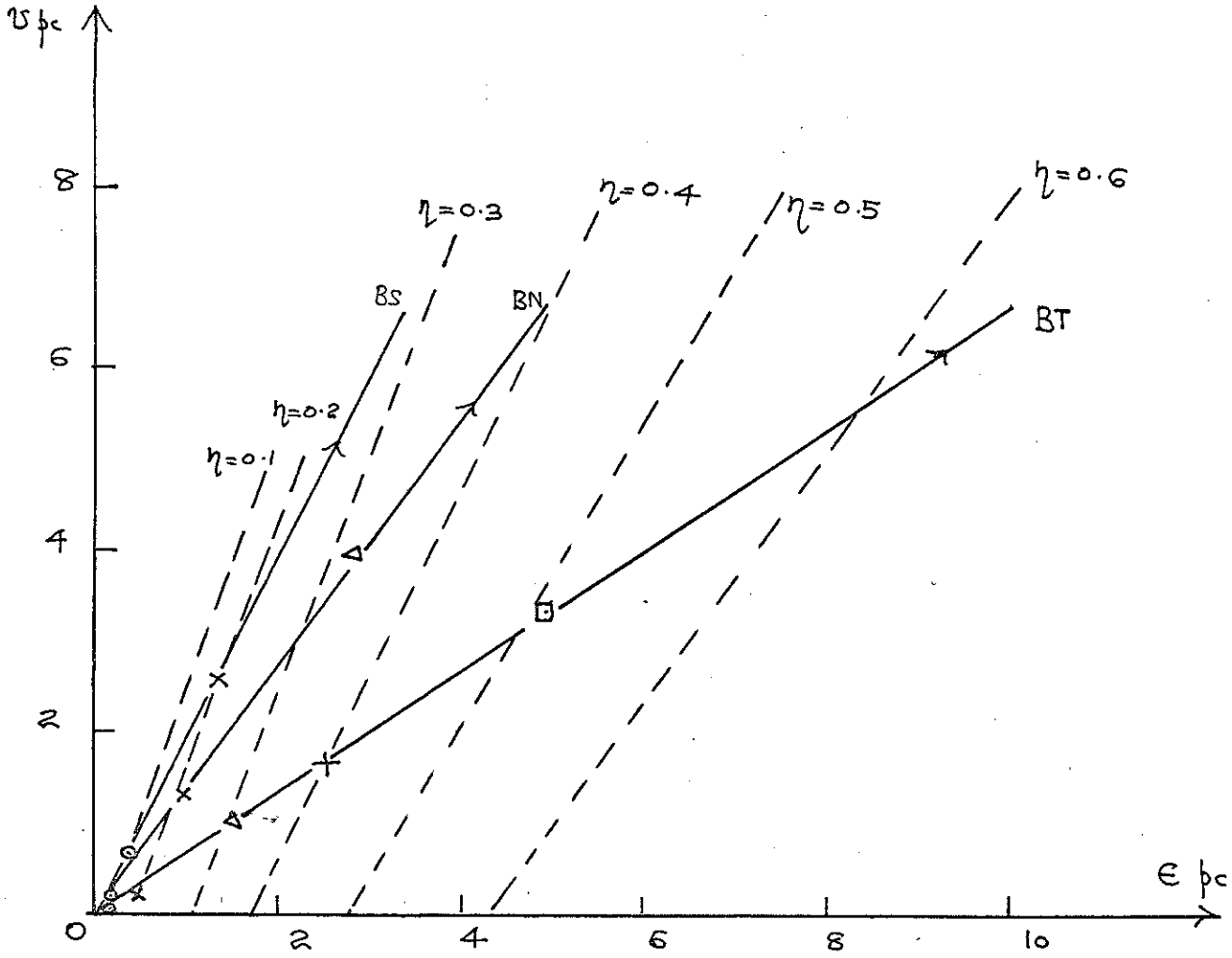

Fig. 7.29. The (υ, ϵ) characteristics of ζ tests BS, BN and BT with contours of constant q/p taken from Fig. 7.3

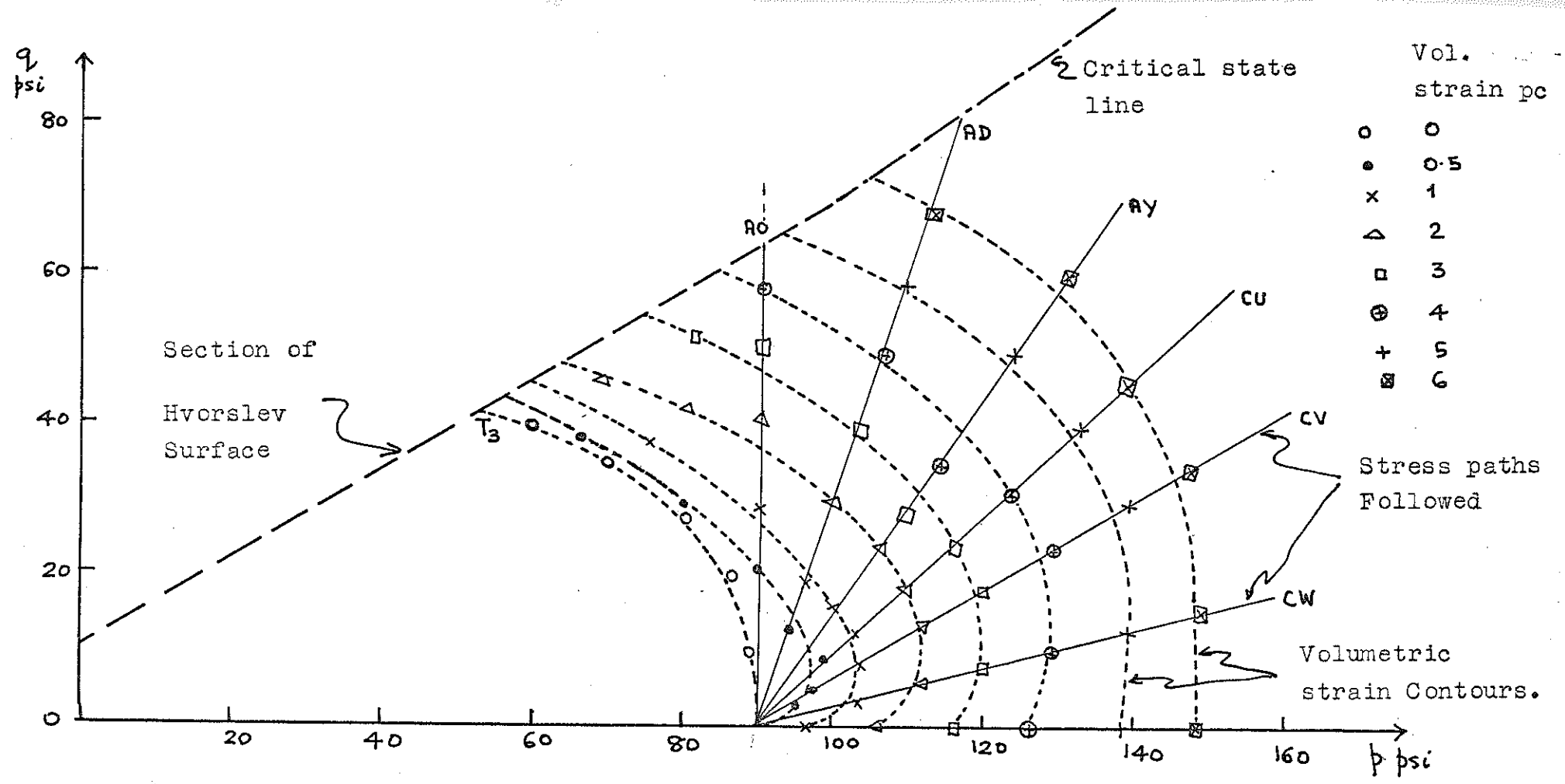

Fig. 7.30 Volumetric strain contours obtained from a variety of drained tests (each with constant dq/dp) and the zero volumetric strain contour from an undrained test.

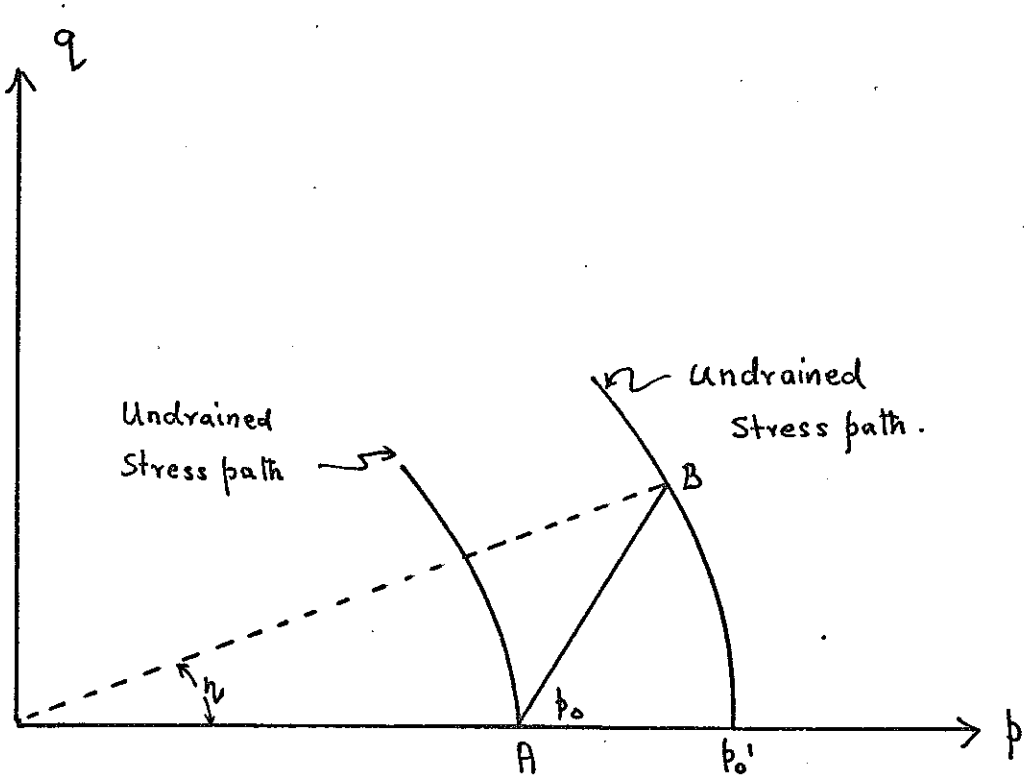

Fig. 7.3I. The similarity of undrained stress paths of specimens sheared from isotropic stresses.

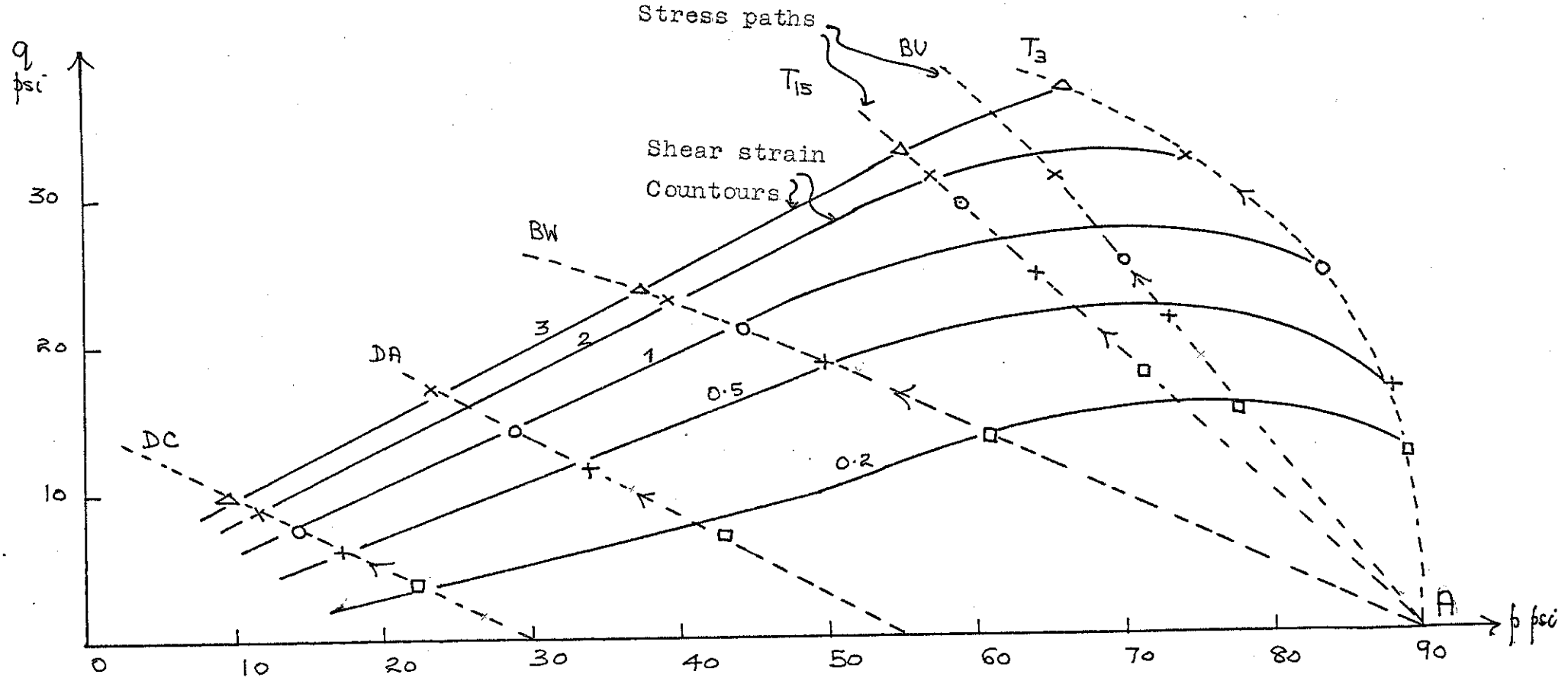

Fig. 7·32. Shear strain contours of specimens sheared along Group 2 stress paths under the conditions $d\eta > 0$ and $dv < 0$

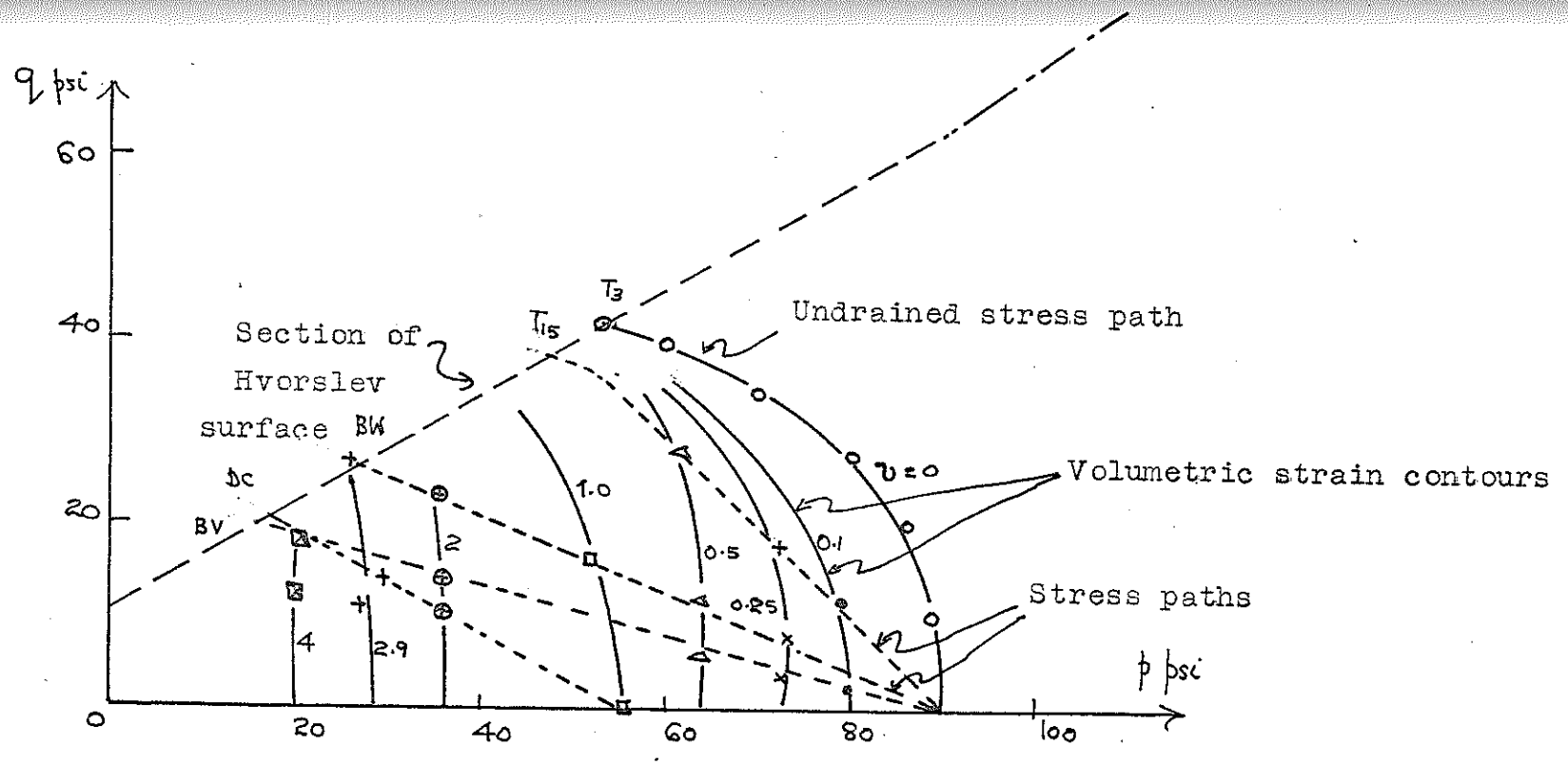

Fig. 7.33. Volumetric strain contours of specimens sheared along Group 2 stress paths under the conditions $d\eta > 0$ and $d\upsilon < 0$

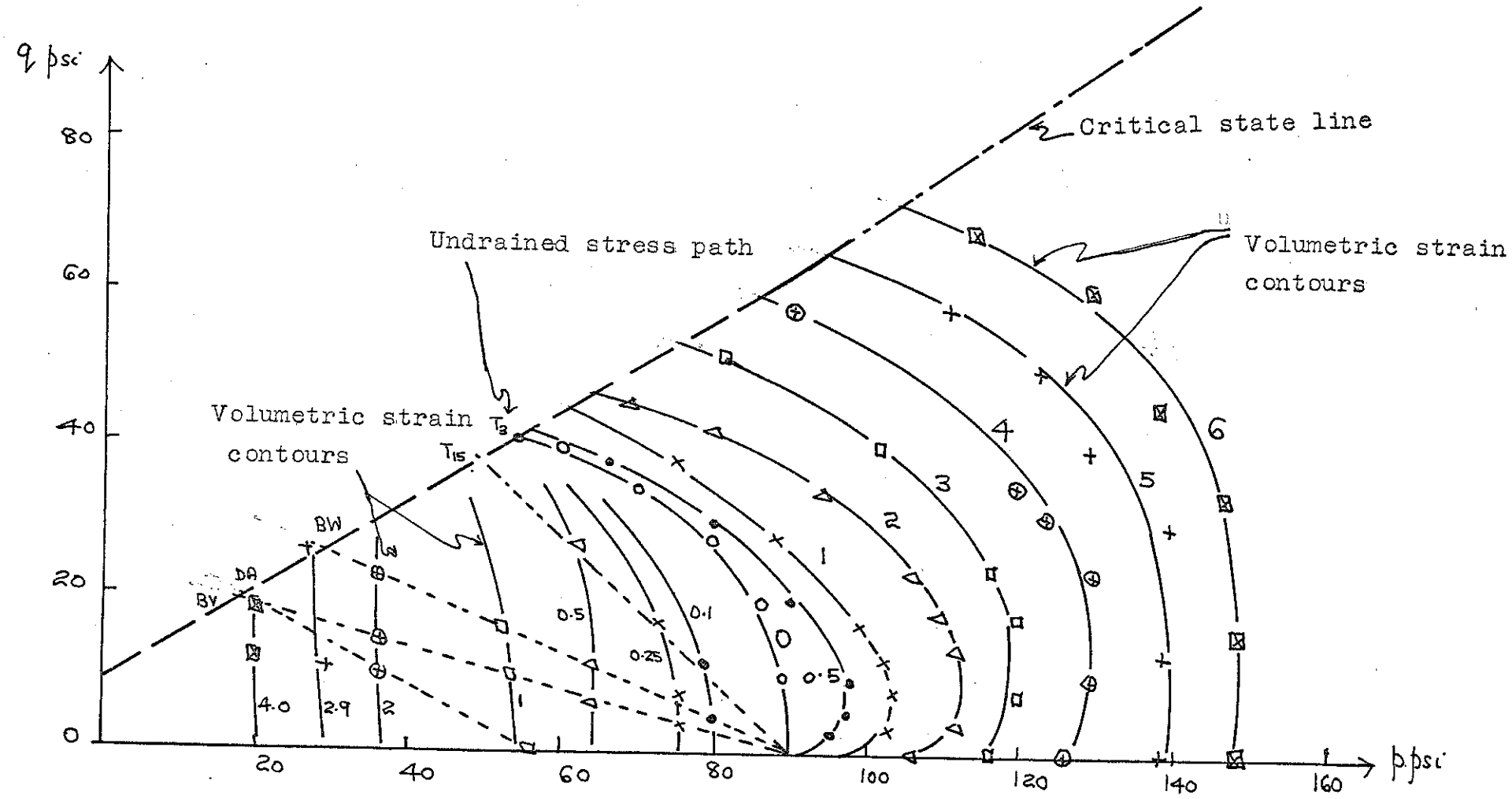

Fig. 7.34. Comparision of volumetric strain contours on specimens sheared along Group I and Group 2 stress paths.

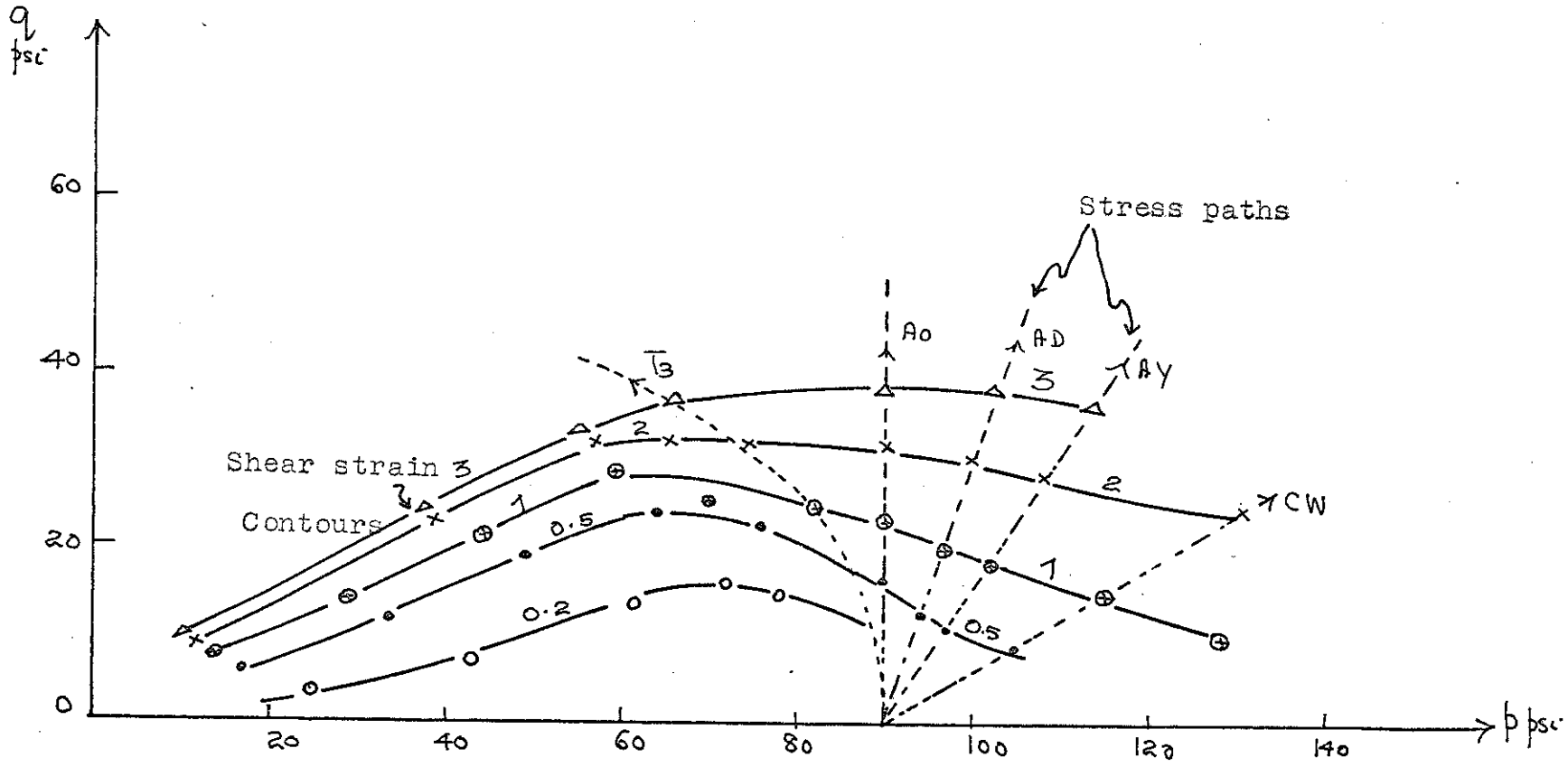

Fig. 7.35. Comparision of shear strain contours of specimens sheared along Group I and Group 2 stress paths.

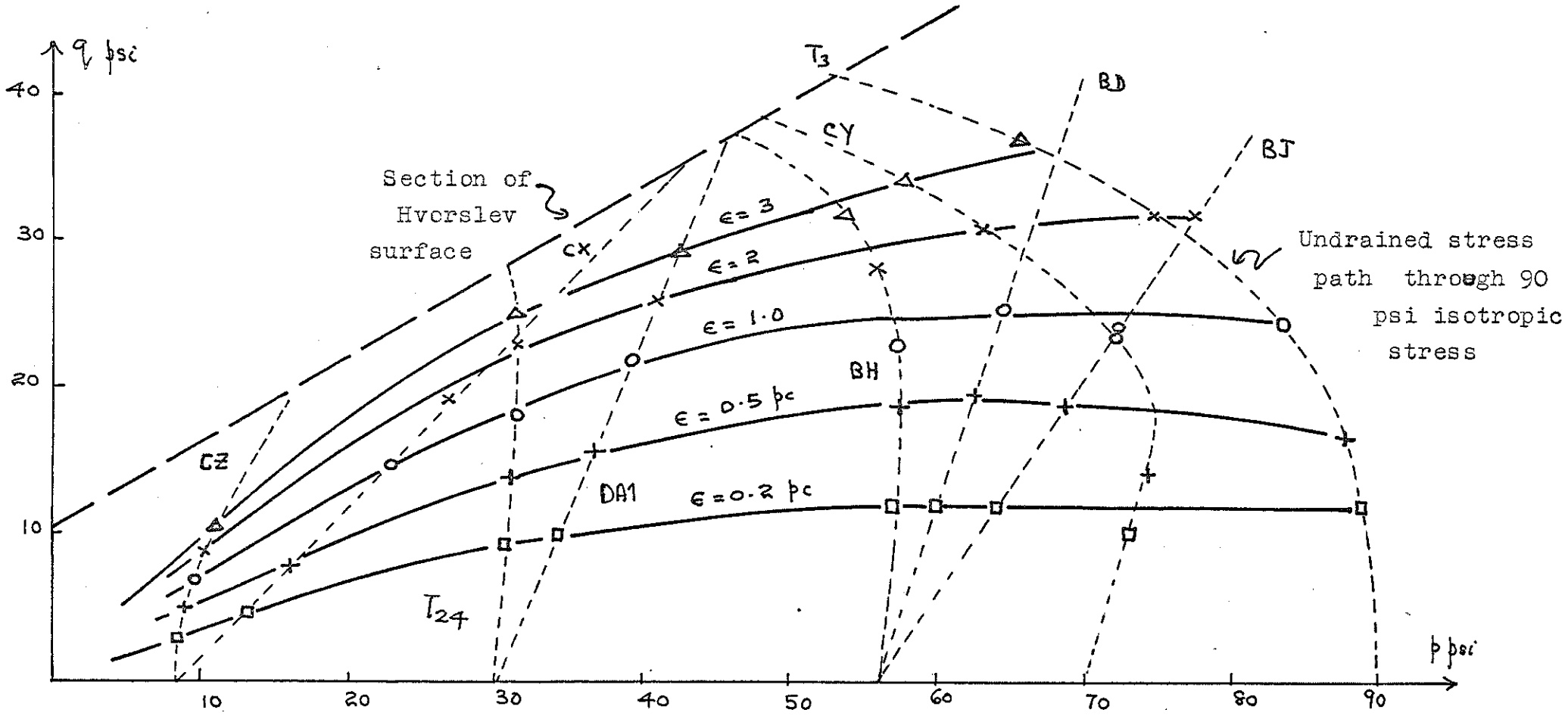

Fig. 7.36. Shear strain contours for specimens sheared along Group 2 stress paths (Type 2) under the conditions $d\eta > 0$, $dv > 0$. (Tests CZ, CX, T_{24}, DAI, BH, CY, BD, BJ and T3)

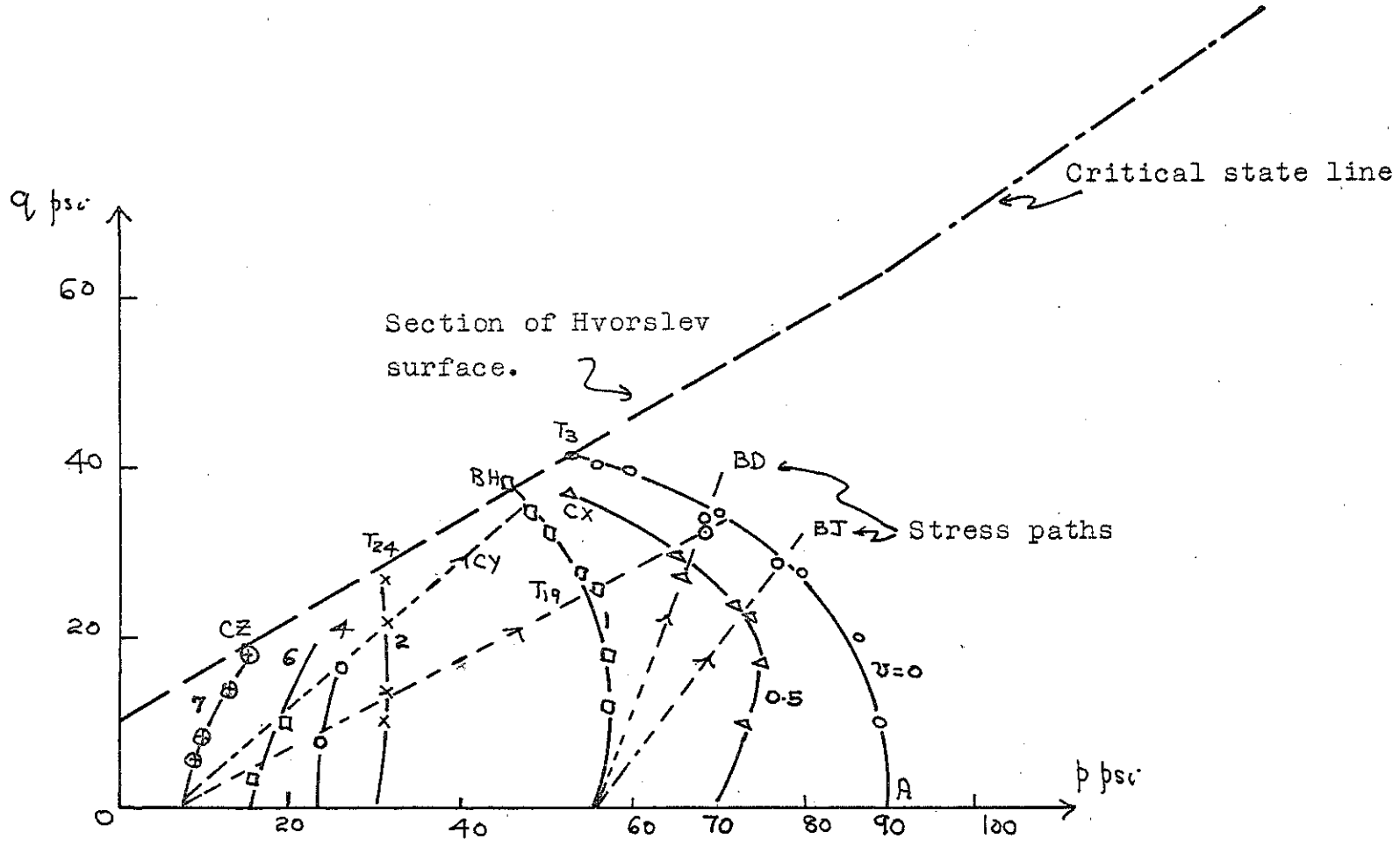

Fig. 7.37. Volumetric strain contours of specimens sheared along Group 2 stress paths under the conditions $d\eta > 0$ and $dv \geq 0$

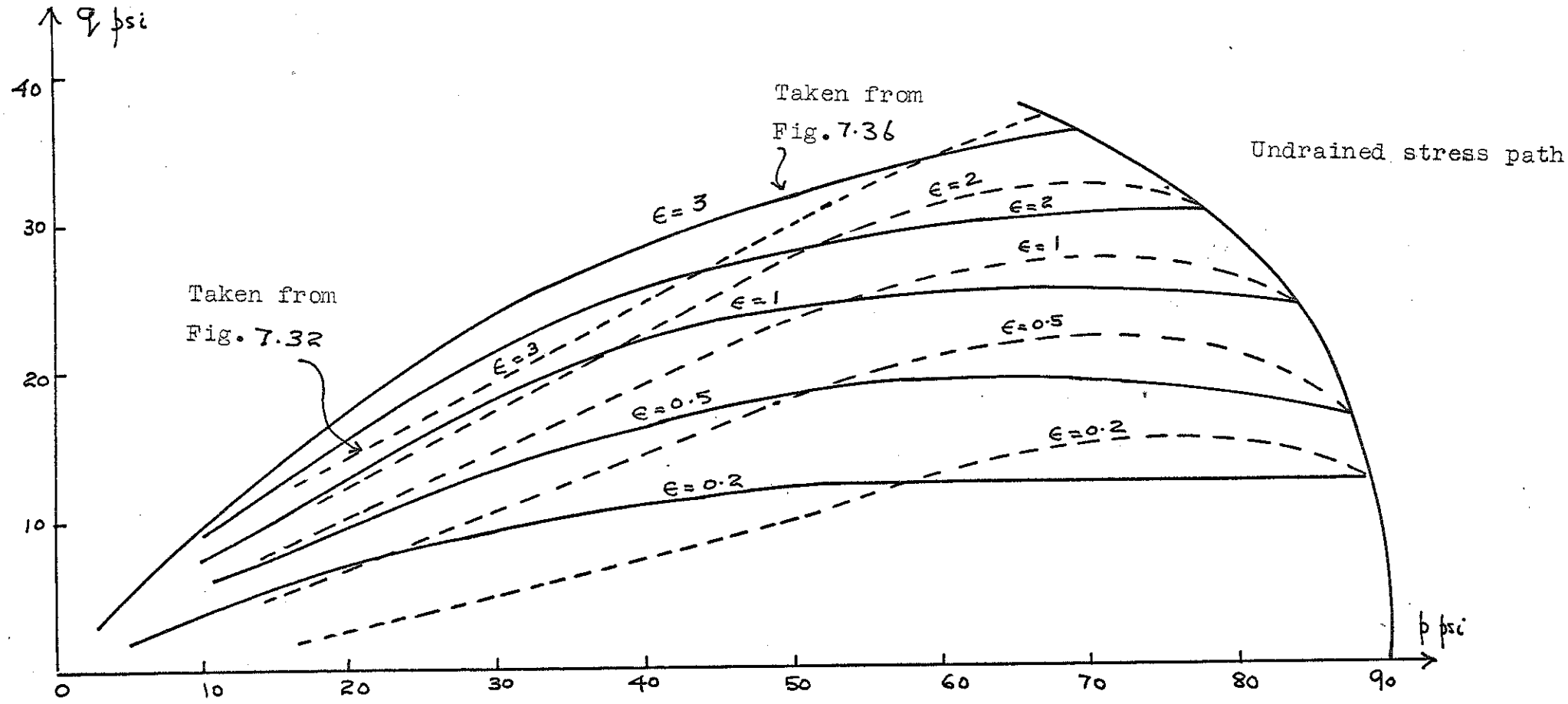

Fig. 7.38. Shear strain contours inside the undrained stress path through 90 psi isotropic stress.
Group 2 (Type 1 and 2)

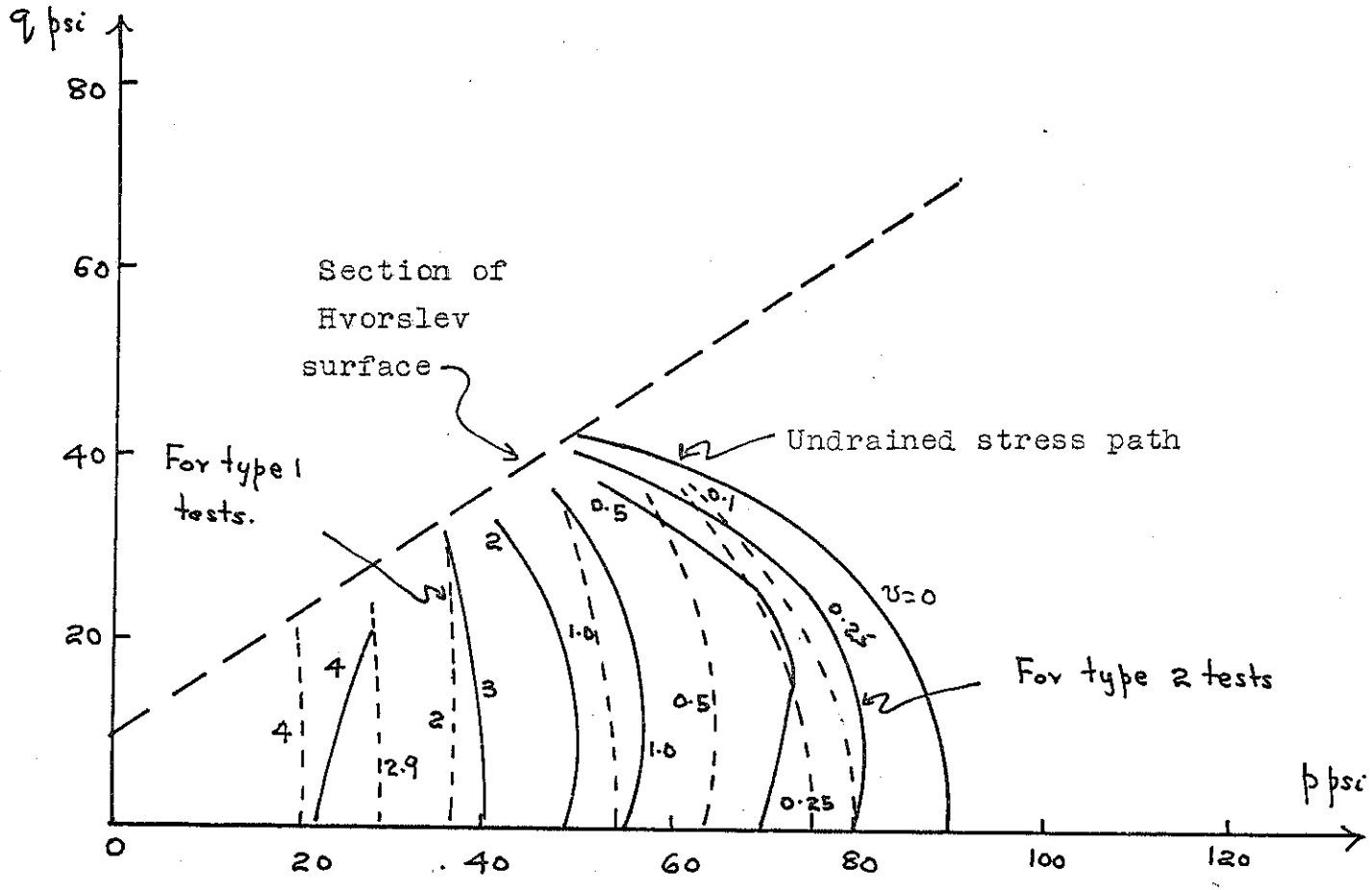

Fig. 7.39. The volumetric strain contours of specimens sheared along Group 2 stress paths (Types 1 and 2), where the state paths lie below the state boundary surface.